

POLITECNICO DI TORINO

Master of Science in Mechatronic Engineering

Master Thesis

**Sliding Mode Attitude Control
for Small Satellite
with Manipulator**



Supervisors:

Dr. Elisa Capello
Dr. Hyeongjun Park

Candidate:

Filippo Caldera

April, 2019

Abstract

Small satellites are making their way into different space missions: from Earth Observation to Space Exploration, the number of less-than-500 kg satellites in space is going to increase. Thanks to their low cost, accessibility and relatively easy to make, small satellites are the choice for a several Universities, research centers and some government agencies. With the advancement in technology, even the space robotics can finally employ small satellites as manipulator carriers. In the past, space robotics was limited to conventional manipulators like Canadarm on the Space Shuttle or other robotic arms mounted on the Mir or ISS only. Such space robots could perform several tasks like inspection, maintenance, assistance, repair and in-orbit assembly.

In the case of assistance, inspection and repair the small satellite could be used to fix other satellites, increasing their lifetime, avoiding the need to launch a replacement and reducing even more the mission's cost. Since one small satellite-based manipulator could assist and fix more than one satellite and, given their relatively modest dimensions and mass, several of them can be place in orbit with one launch vehicle the overall cost saving is very relevant. These new types of missions and small satellites could open a new space business focused in repairs also.

The challenges that arise with small satellites equipped with manipulator are the reactions of the two subsystems that influence each others. Such reactions, in these cases, may be relevant and no more negligible as the case with satellites or spacecraft with bigger dimensions.

These forces, torques and accelerations can affect the attitude precision, which is critical for such applications.

In this thesis, a two-channel control system is proposed to control a small satellite equipped with a manipulator, mounted on top of the satellite. The control objective is to design two separate controllers for the multi-body system, considering two control channels. The main goal is to limit the manipulator's reactions on the base-satellite's attitude trying to achieve the desired attitude with a minimum error. Two Second Order Sliding Mode Controller (SMC) suitably designed, to maintain the desired attitude even when the manipulator is moving. The multi-body model and simulation has been developed in the MATLAB/Simulink environment. Several scenarios have been simulated showing that the two-channel control design is able to track and maintain the desired attitude. Even in the scenarios where both the manipulator and the base-satellite were moving a good tracking has been observed. Hence, a good attitude tracking is guaranteed regardless of the manipulator's reactions.

Sommario

Gli small satellites stanno comparando sempre di più in diverse missioni spaziali: dalle missioni per l'Osservazione della Terra a quelle dell'esplorazione spaziale, il numero di questi satelliti con massa inferiore a 500 kg crescerà. Grazie al loro basso costo, accessibilità e facilità di costruzione, gli small satellites sono scelti da diverse Università, centri di ricerca ed anche agenzie governative. Con l'avanzamento del progresso tecnologico, anche la robotica spaziale potrà finalmente impiegare questi piccoli satelliti come base per bracci robotici. Nel passato, la robotica spaziale era limitata a pochi veicoli o strutture spaziali, come il Canadarm montato sullo Space Shuttle od altri bracci robotici montati sulla ISS o Mir. L'introduzione di manipolatori spaziali ridotti nelle dimensioni, potrebbero rendere compiti come ispezione, manutenzione, assistenza, riparazione ed assemblaggio in orbita più diffusi. Nel caso della assistenza in orbita, gli small satellites potrebbero essere usati per riparare altri satelliti, allungandone la loro vita operativa ed annullando la necessità di lanciare in orbita un sostituto. Questo ridurrebbe i costi di svariate missioni spaziali. Dal momento che la robotica spaziale basata sugli small satellites potrebbe assistere più di un satellite e, data la loro massa ridotta ed il loro ridotto volume, diversi di questi oggetti possono essere portati in orbita con un singolo lancio, riducendo ancora di più i costi. Queste nuove tipologie di missioni per small satellites possono aprire nuove e svariate opportunità nel mercato aerospaziale. Le sfide da considerare con gli small satellites equipaggiati con manipolatori sono le reazioni che questi due sottosistemi applicano uno sull'altro. In questi casi, gli effetti di queste reazioni non possono più essere considerati trascurabili come nel caso di manipolatori montati su grandi strutture. Infatti, queste forze e momenti applicati su un piccolo satellite possono influenzare la precisione d'assetto che, in questi scenari, rappresenta un aspetto rilevante. Questa tesi propone un controllore a due canali per controllare l'assetto del piccolo satellite a cui è stato aggiunto un braccio robotico. L'obiettivo è progettare due controllori separati per il sistema multi-body, considerando i due canali di controllo. Lo scopo principale è limitare gli effetti delle reazioni del manipolatore sull'assetto del satellite base, cercando di ottenere l'assetto desiderato con un errore minimo. Due controllori Sliding Mode (SMC) del secondo ordine sono stati progettati, per mantenere l'assetto del satellite anche quando il manipolatore è in movimento. Il sistema multibody ed il suo controllo è stato sviluppato in ambiente MATLAB/Simulink. Diversi scenari sono stati simulati, mostrando che il controllo a due canali è in grado di inseguire e mantenere l'assetto desiderato. Anche negli scenari dove il manipolatore è stato considerato in movimento, un buon inseguimento dell'assetto è stato osservato. In conclusione, l'inseguimento dell'assetto di reference è garantito a prescindere dai movimenti del manipolatore.

Acknowledgements

I would like to express my sincere gratitude to Dr. Elisa Capello from Politecnico di Torino and to Dr. Hyeongjun Park from New Mexico State University. I am very thankful to Dr. Capello for her kindness, expertise and patient showed in this months.

A sincere thank goes to Dr. Park for his competence, availability and for being a solid reference in a Country new to me. There is no way I can express how much valuable yours advices on both engineering and personal level are. I consider both my advisors as great guides and models to follow and imitate.

Thanks to my father Diego, my mother Franca and my sisters Paola and Samanta for supporting me in all means during this enterprise. A special thanks to $\phi\phi$, for always put up with me, even in the hardest periods, no matter what.

Thanks to my friends, in particular Andrea C. and Andrea T., for offering me their genuine friendship and for sharing some very good memories starting back from High School, passing through University and, hopefully, even in the future.

Lastly, I would like to dedicate this work to my gone grandfathers: Felice and Arnaldo.

Contents

Abstract	ii
Acknowledgements	iii
List of Figures	v
1 Introduction	1
1.1 Overview of the Thesis	7
2 Sliding Mode Control Theory Recalls	8
3 Base-Satellite Model and Control	13
3.1 Base-satellite Model	13
3.2 Reaction Wheels Dynamic Model	16
3.3 Base-Satellite Sliding Mode Attitude Controller	18
4 Manipulator Model and Control	20
4.1 3 DoF Manipulator Model	20
4.2 Manipulator Sliding Mode Control	24
5 Multi-body Plant Dynamics Model	26
5.1 Reference Frames	27
5.2 Equations of Motion	28
5.3 Manipulator Reaction on the Base-Satellite	31
5.4 SPART Implementation	33
6 Simulations Results	36
6.1 Scenario 1	37
6.2 Scenario 2	39
6.3 Scenario 3	42
6.4 Earth-Observation-like Mission	45
Bibliography	50

List of Figures

1.1	Rising trend of small satellites during the past decades. Data from [3]	2
1.2	On-orbit servicing concept. Figure from Astrium	2
1.3	Example of assembling robot proposed by W. Oegerle [10]	3
1.4	Astronaut Christer Fuglesang carries out assembly tasks on the ISS. Credit ESA	4
1.5	Archinaut on-orbit automated concept. Credit NASA/Made in Space [14]	4
1.6	Damaged on solar panels. Credit ESA	5
1.7	NASA's Restore-L concept. Figure from [17]	5
1.8	On-orbit refueling interface concept [19]	6
2.1	General Control System block diagram	8
2.2	Sliding Mode's base concept	9
2.3	SMC phases	10
2.4	switching function $sign(\sigma)$	11
2.5	switching function $tanh(\mu\sigma)$	11
3.1	Base-Satellite Reference Frame J_0	13
3.2	Earth-Spacecraft system	14
3.3	Base-Satellite dynamics and kinematics Block Diagram	16
3.4	Reaction wheels pyramidal configuration. Figure from [26]	16
3.5	Reaction Wheel Block Diagram	17
3.6	Base-satellite model block diagram	17
3.7	Base-satellite attitude controller performances	19
4.1	3 DoF manipulator with 3 revolute joints and two links	20
4.2	Manipulator working space	23
4.3	Manipulator's SMC performances	25
5.1	Examples of J_i (Joint RFs) and \mathcal{L}_i (CoMs RFs)	27
5.2	$J_{r_{0C}}$ representation	29
5.3	$J_{r_{0i}}$ representations	29
5.4	Reactions magnitude and period of action	32
5.5	Denavit-Hartenberg parameters. Figure from <i>Robotics. Modelling, Planning and Control</i> [30]	33
5.6	Manipulator joints and RFs	34
5.7		35

6.1	Quaternions tracking with manipulator holding a constant position . . .	37
6.2	Quaternions tracking error	37
6.3	Euler's Angles	38
6.4	Torque input by SMC controller	38
6.5	Quaternions tracking with moving manipulator and constant attitude . .	39
6.6	Quaternions tracking error	40
6.7	Euler's angle	40
6.8	Reactions	41
6.9	Torque input by SMC controller	41
6.10	Quaternions tracking with moving manipulator	42
6.11	Quaternions tracking error	43
6.12	Euler's Angles	43
6.13	Torque input by SMC controller	44
6.14	Quaternions tracking with moving manipulator	45
6.15	Quaternions tracking error	46
6.16	Euler's angles tracking error and manipulator's disturbances	46
6.17	Satellite's displacement trajectory due to manipulator reactions	47
6.18	Euler's Angles tracking errors comparison	47

Chapter 1

Introduction

The goal of this thesis is to design an attitude controller for a small satellite equipped with a robotic arm. Both the spacecraft and the robotic manipulator are nonlinear systems in terms of dynamics and kinematics, thus the attitude control should ensure high accuracy and robustness against external disturbances and parameter variations. As in [1], a coordinated control between the satellite's attitude control system and the manipulator's control system is proposed. In a similar way in [2], gain scheduling control is proposed to reduce the satellite attitude error caused by the manipulator's motion and showed good performance, providing a good reason to design, for this thesis, a second order Sliding Mode Controller (SMC). This controller is proposed for precise attitude control, in which disturbances are obtained by the arm movement. The main idea is to design a control system able to reduce the manipulator reaction effects, to maintain the desired attitude. This consideration is more relevant when a small satellite is considered.

The term small satellite refers to an object with mass lower than 500 kg. The common features of these objects are the small volume and mass, that allow small satellites to be launched as cargo and later being deployed by an other spacecraft or directly as payload. Given the small dimensions it's possible to place in orbit multiple objects, even different ones, with a single launch vehicle. Since the cost of launch is heavily affected by the payload mass, small satellites offer a relatively low-cost solution to space access.

Small satellites have been in space since the 50s, experienced a boom in the mid-60s and, given the technological advancements allowing to shrink down even more the satellites' dimensions and reducing the production costs, they are experiencing a significant growth during the past decades, as Fig 1.1 shows.

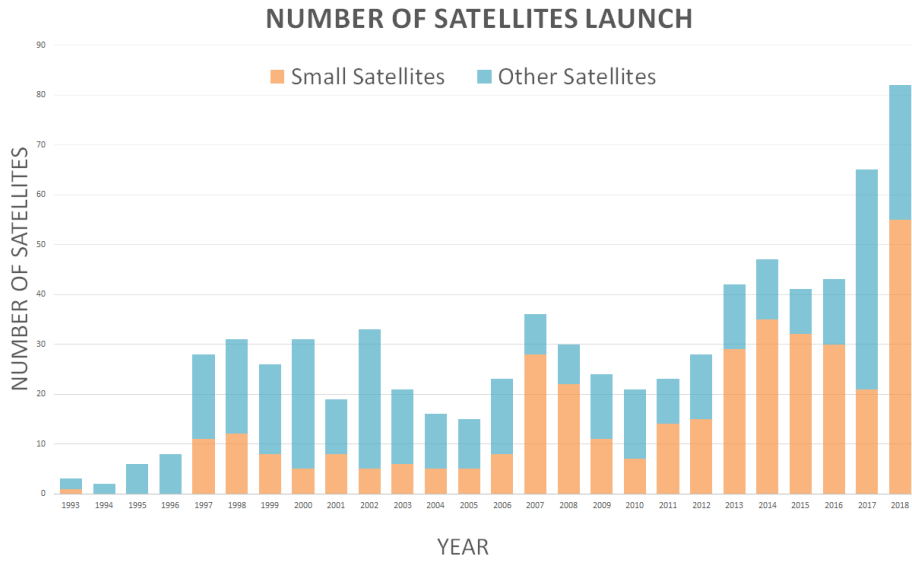


Figure 1.1: Rising trend of small satellites during the past decades. Data from [3]

Most of the small satellites currently in space are for Earth Observation or technological demonstration purposes but some studies about servicing and orbital manipulator have been made as well.

In particular, a small satellite equipped with a robotic manipulator is classified as a free-floating robots (not space robots in order to avoid confusions with rovers and probes used for space exploration). Such system has their design inspired by industrial robots but, despite their similarities, the control systems of manipulators in space have to consider the free-body dynamics due to micro-gravity.

Some studies [4][5][6][7] about on-orbit servicing reports that space manipulator's applications are limitless and include refueling, inspection, upgrade, assistance and on-orbit assembling.

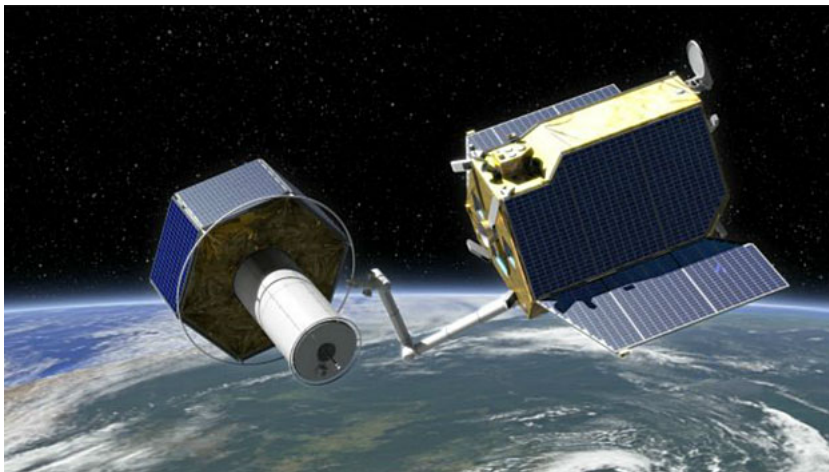


Figure 1.2: On-orbit servicing concept. Figure from Astrium

Currently some big manipulators are already in use as sort of space crane on-board the International Space Station (ISS), used to guide some spacecrafts' docking, perform on-orbit assembling and deploy small satellites. This is the case for the Canadarm II and Special Purpose Dexterous Manipulator, which played a major role in assembling the ISS. The concept of on-orbit assembling consists in combining together pre-fabricated structures in order to actually built a bigger structure [8][9]. This procedures derive also by the limited volume of the payload bay inside a launch vehicles; such payload volume is unlikely to be increased in the next generation of launch vehicles. There is a mission concept [10] proposing a 30m aperture space telescope to be placed in the Sun-Earth Lagrangian Point 2 orbit. Due to the difficulties to operate in such orbit the concept is to assemble this telescope in the Earth-Moon Lagrangian Point 2 and, once completed, move it where intended to. Given the large structure, all the parts and components would not fit in a single launch vehicle so they would be delivered with three separate launches.

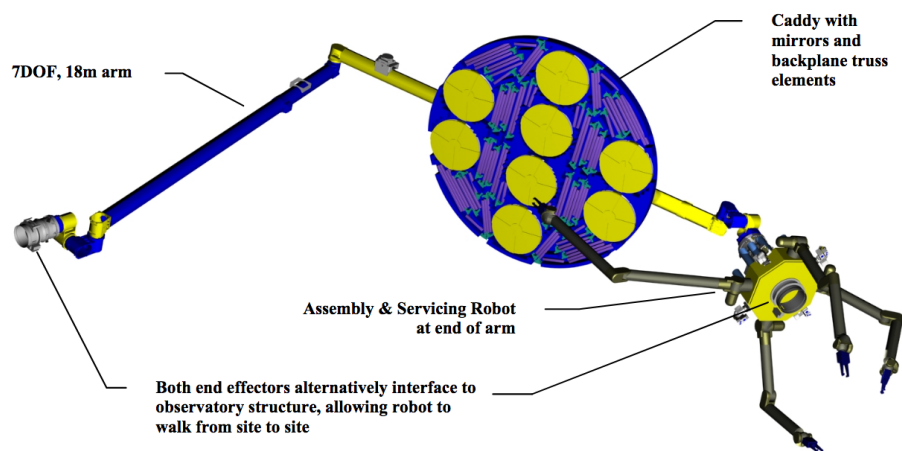


Figure 1.3: Example of assembling robot proposed by W. Oegerle [10]

An orbit assembling would required higher precision and a smaller working zone that the big manipulators like the ones stated in the previous lines might not have. Hence, smaller space manipulators are also required. Akin in *Lightweight Modular Self-Reconfigurable Robotics for Space Assembly, Inspection and Servicing* [11] provides some conclusions and requirement concerning such miniaturize robotic manipulators. In the specific, the orbital manipulator should have 6 degree-of-freedom in order to perform most of its operations in the real world space, needs to have a limited mass while maintaining its length over one meter at least. An important requirement is the power consumption. Since those items are very likely to be carried by a small spacecraft, their power consumption, including their actuators and controls, has to be limited. A good estimate would be to have a total power requirement less than 100W. Other requirements are related with modular and reconfiguration capabilities while on orbit, in order to increase the manipulator abilities and versatility. Considering the versatility aspect, the manipulator End Effector has to be designed in such a way it can host several tools and, thus, being able to perform different task, requiring different tools.

Still in the assembling case, S. Eckersleya in *In-Orbit Assembly of Large Spacecraft Using Small Spacecraft and Innovative Technologies* [12] suggests to employ multiple small manipulators, formed by cooperating units able to perform more complex on-orbit assembling. Using

this idea, the advantages are that a considerable and possibly more articulated structure may be build. All these new concepts may open new mission scenarios focused on in-space robotic manufacturing, in the sense of the term including fabrication, assembly and integration [13]. A notable mention to a company, Made in Space [14] that is designing and developing some concept of satellites with 3D printing capabilities. This concept would definitively bring the additive manufacturing to a new, higher level and open new frontiers in space manufacturing.



Figure 1.4: Astronaut Christer Fuglesang carries out assembly tasks on the ISS. Credit ESA



Figure 1.5: Archinaut on-orbit automated concept. Credit NASA/Made in Space [14]

Considering the inspection, repair and upgrades aspects, a satellite with manipulators would be required to perform such missions. Nowadays the satellites that have been upgraded while in orbit are just few handful but, as predicted in [3], the number of satellites launches is in constant grown and opens the discussion of possible future missions and scenarios. With such increasing number of potential customers, repairs missions could be possible in the future. Usually, a satellite is disposed when its mission is completed, its lifetime is about to end or because it becomes faulty. As explained in [15], a spacecraft fails mostly because of the space environment or some failures in the spacecraft's components. Considering the space environment, the Sun creates plasma-induced electric charges that could cause a strong and potentially damaging electric stress on the spacecraft. In facts, the number of faulty spacecraft because such discharges is depending on the solar cycle. There are other common random failures, considering the spacecraft design, that may happens anytime during the spacecraft's lifetime. A faulty component does not represent an issue in most of the cases because satellites and spacecraft are equipped with high quality components. There is redundancy in their design but, since the space debris constitute an serious hazard, the scenario where a satellite is damaged is most likely. Such a problem isn't new and a United Nations report dated back from 1999 [16] reported that, at that time, the average collision time with a 1cm debris for a 10m^2 cross-section area satellite may be just three years for certain orbits. Since the space debris situation has worsened in 20 years and a satellite usually spent 15 year in orbit, the debris impact is almost a certainty. As Fig.1.6 suggests, an example could be the replacement of solar panels, which are the largest surfaces in solar powered satellite.

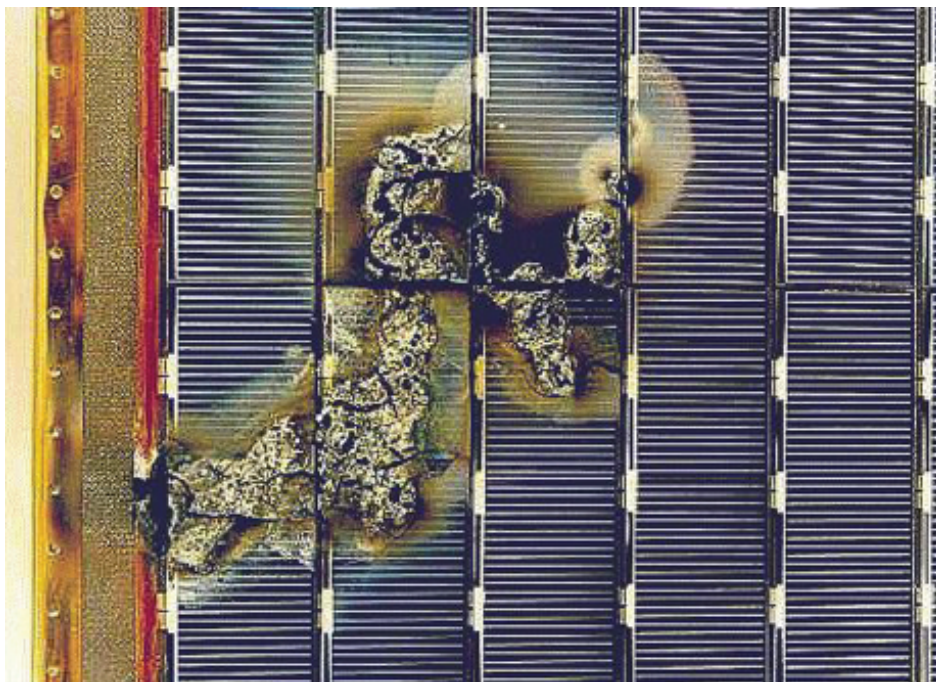


Figure 1.6: Damaged on solar panels. Credit ESA

Some missions have been studied. For instance, mission from NASA, using the Restore-L spacecraft, is planned to take place in 2022 [17].

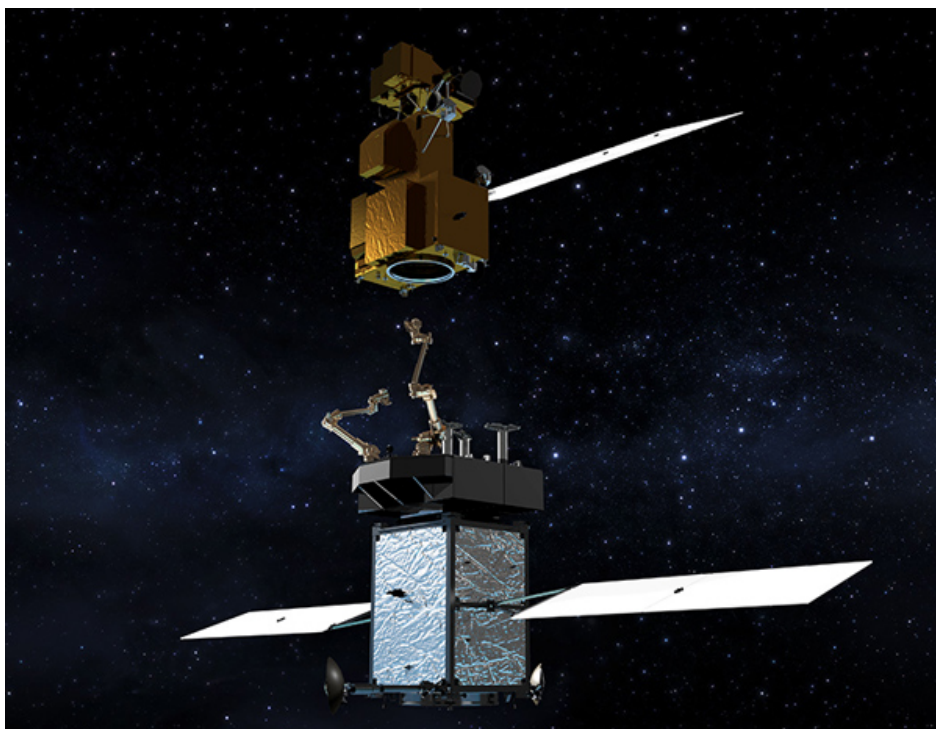


Figure 1.7: NASA's Restore-L concept. Figure from [17]

Other mission scenarios for space manipulators are the cases for De-Orbiting or Re-Orbiting a satellite [15]. Considering the scenario where a launch vehicle fails and the payload is placed in an orbit that it's not the intended one, a Re-Orbiting mission would consist in reaching and docking the customer and carry it on the right orbit. A interesting mention comes from B. Sullivan, [18] (Table 7.13) stating that, on average, once a year a high valuable spacecraft planned to be in geosynchronous orbit, fails to reach the orbit, dooming the investment and revenue. In a different scenario, where a satellite is needed to vacate an orbit is cruising, a De-Orbiting mission can assist the customer satellite in the orbit's change and guide it, for example, into a graveyard orbit or in an atmospheric re-entry, even.

Finally, another use of these small satellites in the servicing domain is refueling. In 1984, Space Shuttle's STS-41G mission has shown that orbital refueling is possible: whit an astronaut Extravehicular Activity, a propellant line was plugged into the payload tankers' valves and the hydrazine transfer has been accomplished successfully and, at these present days, the ISS is refueled on a regular basis using an automated process involving a fluid coupling system embedded in the docking mechanism. For all those satellites and spacecraft designed to be refueled but lacking of such fluid coupling mechanism, a manipulator could be used to connect the transfer line and actuate the valves. Some methodologies are under studies, including a sort-of supply probe or a complete replacement of the propellant tanks. Both of these options involves the use of robotic arms [19].

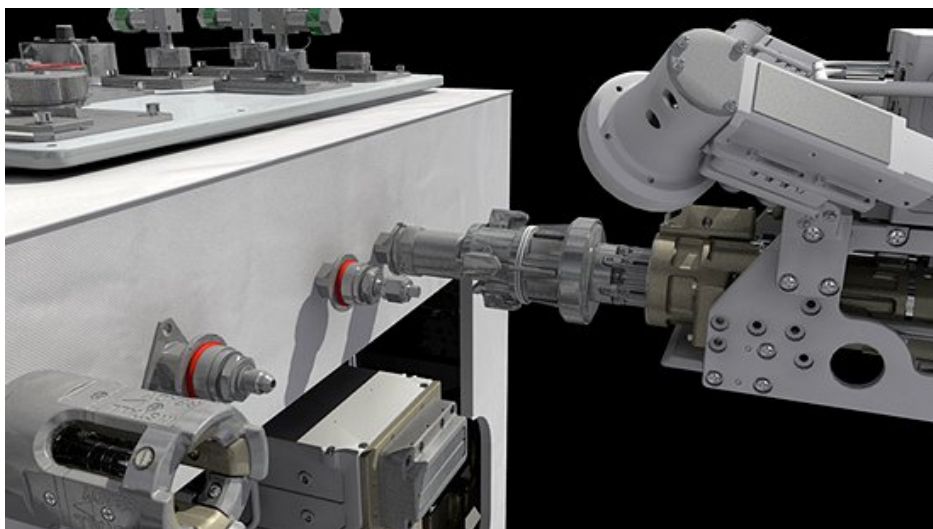


Figure 1.8: On-orbit refueling interface concept [19]

Refueling in space would also help to extend both the mission and satellite's lifespan [20].

At the current level of technology, all the tasks described can be achieved with a certain level of automation, autonomy planning, decision making, perception and grasping capabilities likely to be reached and improved in the nearest future. At these days, most of the robotic performance are overseen by human operators but, given the growing needs and advancements in automation technologies, fully-automated tasks are probably on the horizon.

A relevant aspect to be considered is the economic analysis and challenges. Satellites are complex systems without constant maintenance, repair and upgrade. This leads to expensive designs to make the system lifetime's longer and when a satellite is faulty, it's usually disposed and replaced with another launch. A simple cost analysis about orbit servicing can be comparing the cost of replacing a system, considering the new satellite design, built and launch costs, with the cost of a servicing mission. An example mentioned in the NASA's *On-Orbit Satellite Servicing Study Project Report* [6] is the Orion 3, a communication satellites which, due to an incorrect orbit, failed the mission. The satellite and launch costed around \$ 230 millions and the operational revenue per year should have been \$ 43 million. Since Orion 3 was designed to last 15 years, the total loss was around \$ 645 million.

Using a cost-per-year approach, has been computed [6] that a service satellite must extend the lifespan of at least 50% thought refuel, repair and upgrade three to five customer satellites to be cost-effective. It's better to underline that, in some cases, the repair mission may have be worth it, based on non-economic factors as well.

In conclusion, there are large number of satellites that could be economically viable to service.

1.1 Overview of the Thesis

This thesis suggest a control solution, using the SMC, to be used on a 200kg small satellite with a 20 kg, 3 Degree of Freedom (DoF) manipulator.

The system to be considered is a multi-body system, defined as such because two dynamic entities (manipulator and satellite), with their own dynamics rules are combined together. Having such a system makes the modeling and control design harder. In this thesis the idea to deal with this complex system is to model the entire multi-body plant but design two separate controllers, one for the base-satellite and one for the manipulator.

Some preliminary descriptions about the Sliding Mode Control used in this thesis are presented in Chapter 2. This preliminary discussion of the SMC is needed to understand the control design presented in Chapter 3 and 4.

In Chapter 3, a model and control of the base-satellite is obtained and validated using the Euler's rotation equations and quaternions.

In Chapter 4, the same is done for the manipulator. Starting from the two-link pendulum-like model from literature, the three DoF manipulator's model is obtained and a controller, in the joints' space, is designed and validated.

A description of the entire multi-body system is obtained using the Lagrangian Approach in Chapter 5 and, using the controllers designed in Chapters 3 and 4, the entire system is controlled.

In Chapter 6, several scenarios are considered with different combinations of the two moving systems in order to evaluate the overall control performances. An Earth-Observation mission is simulated as well just to verify the performances with more realistic maneuvers.

Chapter 2

Sliding Mode Control Theory Recalls

As stated in the previous pages, this thesis propose a Sliding Mode Control (SMC) as solution to both base-satellite and manipulator control problem. Both the base-satellite and manipulator considered in this thesis belong to the non-linear system family. To control non-linear plant' models, the Sliding Mode Control is a widely used and well-established. Along being one of the most common choice for non-linear systems, the SMC shows some very nice noise-rejection and robustness properties.

A general control system architecture, adopted in this thesis, is shown in Fig.2.1.

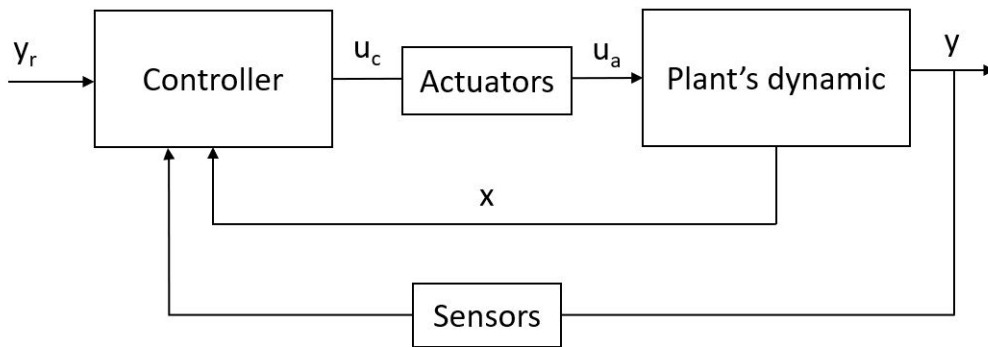


Figure 2.1: General Control System block diagram

Where y_r is the reference signal, y is the actual output of the plant, x is the plant's state, u_c is the command signal and u_a is the input signal of the plant.

In this work of thesis some assumptions have been made:

- Sensors and actuators are considered as ideal ones. Thus, they are considered with infinite bandwidth. For simplicity, sensors are considered with unitary gain while the actuators are modeled in Section 3.2.
- Considering tracking control problem. Hence, the goal of the control design is to satisfy the following condition: $y(t) \rightarrow y_r(t)$, for $t > t_r$, t_r finite.
- State of the plant x are observable. In practise, that means that the physical values constituting the plant's state are measurable. If the state is not observable, an observer is usually employed.

The SMC concept consist in having a sliding surface σ , where the control forces the system's trajectory to reach and slide on it. Imagine the sliding surface dividing a geometric space in two subspaces: $\sigma > 0$ and $\sigma < 0$. the basic idea is to have the system trajectory pushed up (when in the $\sigma < 0$ subspace) or down (when in the $\sigma > 0$ subspace) in order to make it reach and stay on the surface σ .

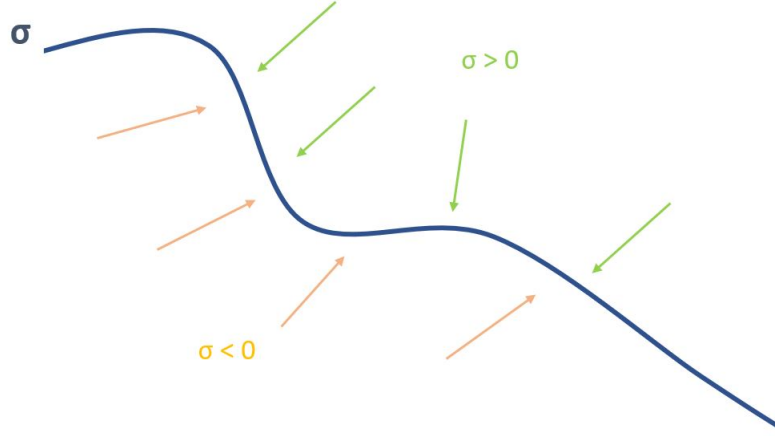


Figure 2.2: Sliding Mode's base concept

There are several typologies of SMC, in this thesis the Second Order Conventional Sliding Mode Control [21] is employed; it allows to exploit the known plant dynamic and introduce it into the sliding surface σ . In this type of SMC, the sliding surface σ is defined as a linear combination of the derivative of the tracking error $e = y_r - y$.

$$\sigma = e^{(\gamma-1)} + k_\gamma e^{(\gamma-1)} + \dots + k_2 e \quad (2.1)$$

The terms k_i have to make all the roots of polynomial $P(x)$ to have negative real part.

$$P(x) = x^{\gamma-1} + k_\gamma x^{\gamma-1} + \dots + k_2 \quad (2.2)$$

Since the SMC, in this case, is a second order one, then $\gamma=2$. Considering a general dynamic system in (2.3)

$$\begin{cases} \dot{x}_1 = x_2 \\ \dot{x}_2 = u + f(x_1, x_2, t) \\ y = x_1 \end{cases} \quad (2.3)$$

defining the output error as $e = y_r - y$ where y_r is the output reference signal, the sliding surface σ is defined as:

$$\sigma = e + c \dot{e} \quad (2.4)$$

Computing the derivative of the sliding surface and highlighting \ddot{y} from (2.3)

$$\begin{cases} \dot{\sigma} = \ddot{e} + k_1 \dot{e} = \ddot{y}_r - \ddot{y} + k_1 \dot{y}_r - k_2 \dot{y} \\ \ddot{y} = \ddot{x}_1 = \dot{x}_2 = u + f(x_1, x_2, t) \end{cases} \quad (2.5)$$

the final form of the sliding surface is:

$$\dot{\sigma} = \ddot{y}_r + k_1 \dot{y}_r - f(x_1, x_2, t) - k_1 \dot{y} - u = \lambda(y, \dot{y}, t) - u \quad (2.6)$$

All the terms in (2.6) coming from the system's dynamic except u are collected in $\lambda(y, \dot{y}, t)$, defined as the cumulative disturbances term. Considering a real dynamic system it's plausible that the cumulative disturbances is bounded, thus $\lambda(y, \dot{y}, t) \leq A$, A finite.

When the trajectory is lying down on the sliding surface (i.e. $\sigma = 0 \rightarrow \dot{\sigma} = 0$), because of the negative real part roots of $P(x)$, $e \rightarrow 0$ exponentially. Hence, the system's input u has to be designed in order to drive the system's trajectory on the sliding surface σ . In the conventional SMC such term is defined as:

$$u = \rho \operatorname{sing}(\sigma) = \begin{cases} -\rho & \sigma > 0 \\ \rho & \sigma < 0 \end{cases} \quad (2.7)$$

The term u (2.7) assures that:

- If the trajectory is not on the sliding surface, it's forced towards the sliding surface σ until reached.
- Once the trajectory reaches σ , the trajectory remains on the vicinity of σ .

These two points represent the two phases of the SMC: Reaching Phase and Sliding Phase. Rarely the initial state of the system is already on the surface, hence it has to be force on it: this is the Reaching Phase. As long the sliding surface is reached, the control law assure that the trajectory of the systems slides along the surface: performing the Sliding Phase. Both phases are graphically shown in Fig. 2.3

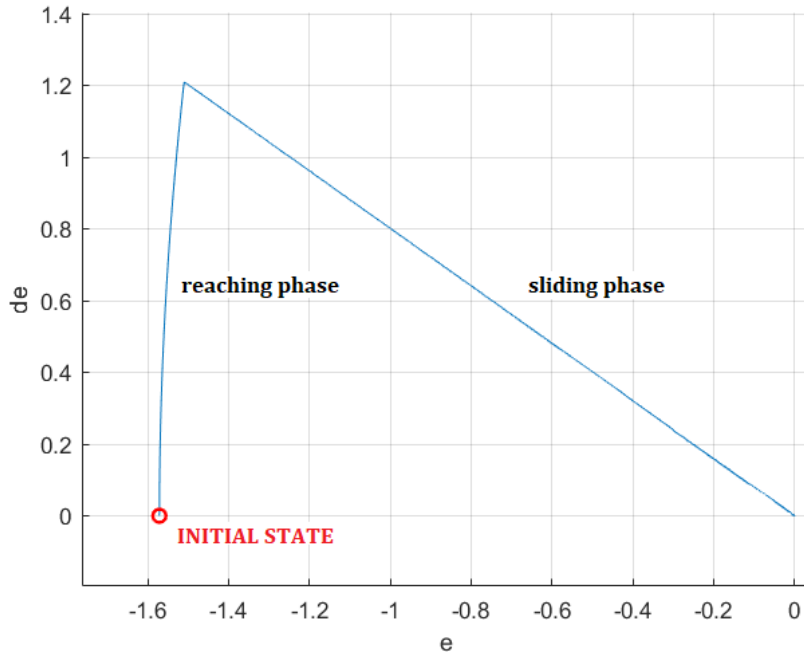


Figure 2.3: SMC phases

One issue of using the $sign(\sigma)$ as switching function is its discontinuity, producing the chattering phenomena Fig. 2.4b in the sliding phase due to an high frequency command activities with limited amplitude Fig. 2.4a in the vicinity of the surface.

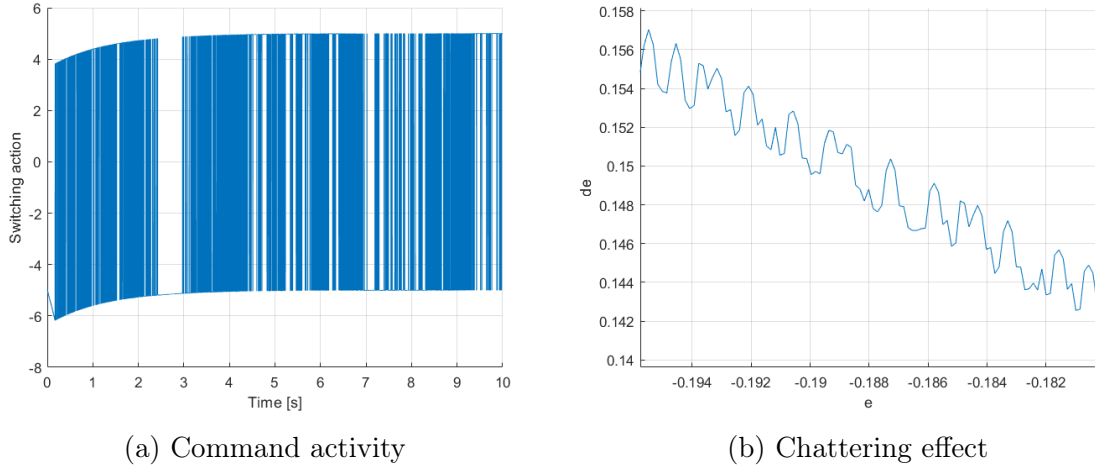


Figure 2.4: switching function $sign(\sigma)$

A commonly used solution to avoid such issues is choosing a continuous switching function [22] at the price of a little performances deterioration. There are several good replacements for the $sign(\sigma)$ function but in this thesis the $tanh(\mu\sigma)$ is employed. The term μ can be exploited to squeeze or extend $tanh(\mu\sigma)$ as Fig. 2.5a shows.

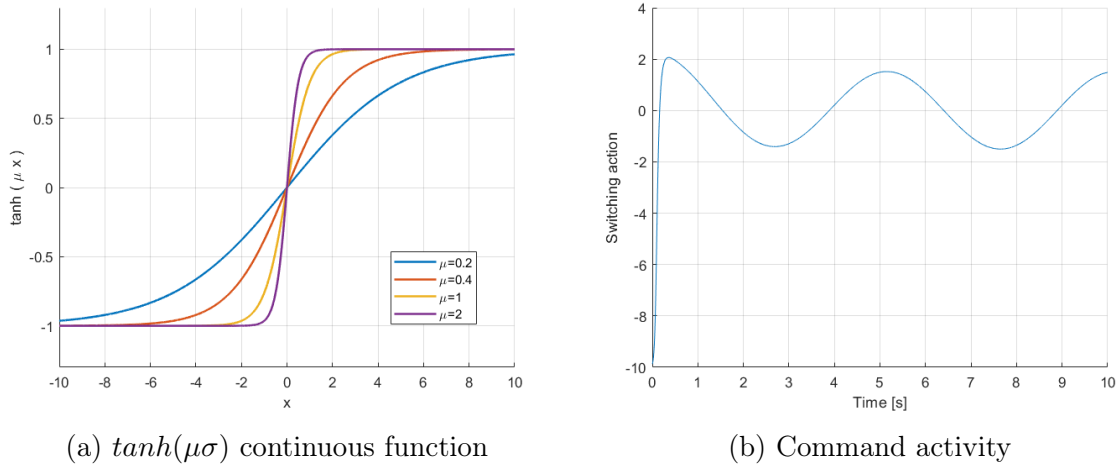
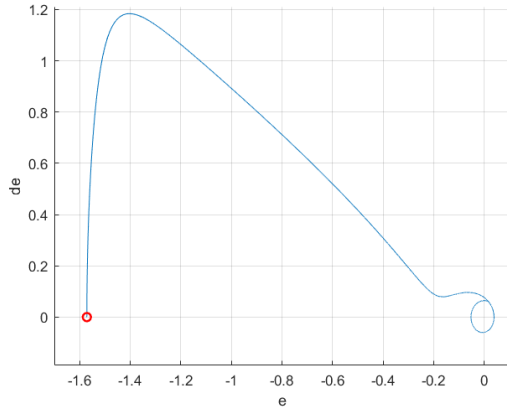
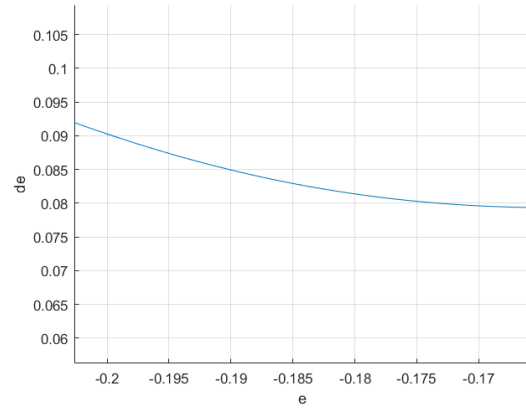


Figure 2.5: switching function $tanh(\mu\sigma)$

Using a continuous switching function, the command activity results to be more relaxed and unbroken than the previous one, as can be seen in Fig. 2.5b. Having a command activity such relaxed leads to a eliminate the chattering issue that affect SMC using the classic switching function.



(a) System Trajectory



(b) Sliding on surface σ without chattering

Chapter 3

Base-Satellite Model and Control

In this chapter the base-satellite is modeled considering the Euler's equations of rotation and quaternions.

This base-satellite is assumed to be equipped with Reaction Wheel (RWs), as attitude actuators while no thrusters are present. After the models of the satellite, its reaction wheels and disturbances are derived, a Sliding Mode Attitude Control is design and simulated.

3.1 Base-satellite Model

Considering the base-satellite as a rigid body, with it's body Reference Frame J_0 reported in 3.1, it's attitude dynamics could be completely described by the Euler's equations [23].

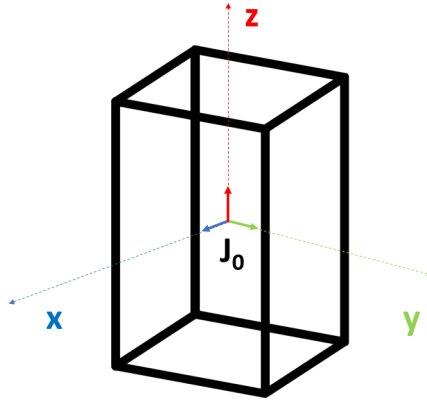


Figure 3.1: Base-Satellite Reference Frame J_0

$$I_s \dot{\omega} = -\omega \times I_s \omega + (M + M_d) \quad (3.1)$$

The term ω indicates the angular rate of about the principal axis. I_s is the body inertia matrix, expressed in the base-satellite frame J_0 and defined, in this case, as:

$$I_s = \begin{bmatrix} I_{xx} & 0 & 0 \\ 0 & I_{yy} & 0 \\ 0 & 0 & I_{zz} \end{bmatrix}$$

where I_{xx} , I_{yy} , I_{zz} are the moments of inertia with respect to the J_0 axis.

Lastly, the terms $M + M_d$ represent the total torque applied to the body, including the torque disturbance terms represented by M_d .

As explained in [23], there are several external torques from different sources acting on an spacecraft in orbit: gravity-gradient torque, magnetic torque, aerodynamic torque and solar radiation pressure. These actions, from a control point of view, could be exploited for better stability of the system or considered as disturbances. In this work, the disturbance case is considered, thus they are considered as terms collected in M_d . Among all these disturbances, this work considers the gravity torque only while the rest are considered negligible.

Considering a spherical gravity gradient and a diagonal inertia matrix of the body, the gravity torque can be described using the inertia moments on the main axes [24]:

$$M_g(R) = \frac{3GM_E}{|R|^5} \begin{bmatrix} (I_{zz} - I_{yy}) R_2 R_3 \\ (I_{xx} - I_{zz}) R_3 R_1 \\ (I_{yy} - I_{xx}) R_1 R_2 \end{bmatrix} \quad (3.2)$$

Where $GM_E = 3.986 \times 10^{14} \text{ m}^3 \text{ s}^{-2}$ is the geocentric gravitational constant [25] and $R = [R_1 \ R_2 \ R_3]$ is the distance from the Earth's center to the Center-of-Mass (CoM) of the orbiting system. In Fig 3.2 are also shown the vectors starting from the system CoM and pointing the individual masses but, since $R \gg r_i$, they're neglected.

Approximating the Earth as a sphere with radius $R_E = 6.371 \times 10^6 \text{ m}$ and defining the altitude from sea-level as R_a it's possible to express R as $R = R_E + R_a$.

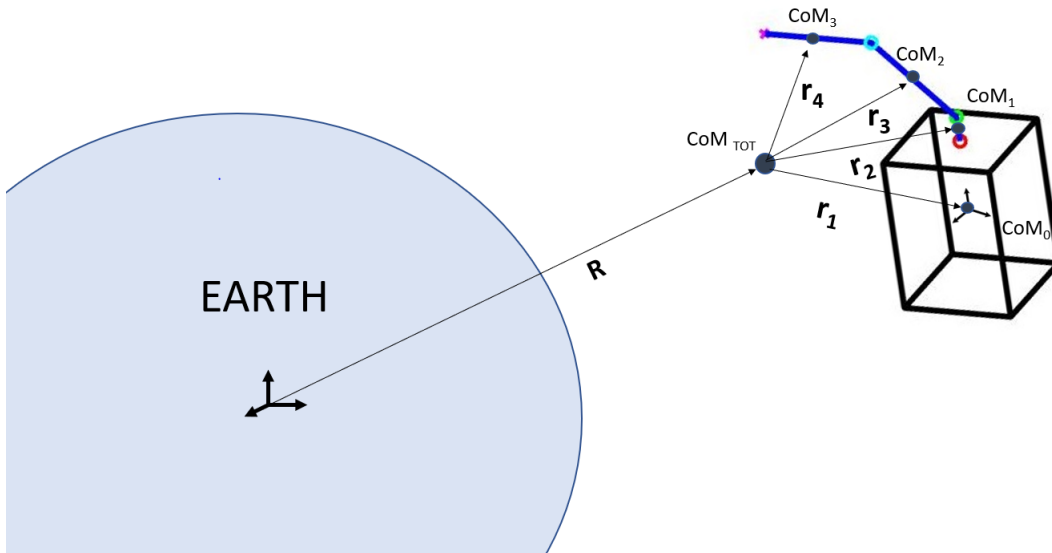


Figure 3.2: Earth-Spacecraft system

Since a servicing spacecraft, like the one considered in this thesis, is expected to operate on different orbits, the worst-case scenario for the gravity torque is considered. The highest gravity disturbances occur in the lowest orbits. Hence:

$$|M_g(R)| \leq |M_g(R)|_{max} = |M_g(R_{min})| \quad (3.3)$$

Given (3.2), the lowest altitude for Low Earth Orbit (LEO) is approximately 200 km, thus $R_a = 2 \times 10^5 m$. Submitting this values in (3.2), the maximum values $|M_g(R)|_{max}$ for the gravity disturbances is around $2 \times 10^{-6} Nm$ in magnitude.

There are also some internal torque disturbances, given by the non-ideal RWs and other non-ideal components but they are not considered in this work. An additional consideration has been made in Section 5.3 about the manipulator disturbances.

In order to avoid singularities that may occur using the Euler's angle attitude representation, unit quaternions q are employed [23]. A quaternion is composed by a real part q_0 and by a vector part q_{123} , in this thesis the format used is the one with the real part placed at the beginning of the quaternion, thus $q = [q_0 \ q_{123}]^T$.

It's possible to express the body's rotations and attitude considering the rigid body's angular rate using (3.4).

$$\dot{q} = \frac{1}{2}O(\omega)q \quad (3.4)$$

where:

$$O(\omega) = \begin{bmatrix} 0 & -\omega_1 & -\omega_2 & -\omega_3 \\ \omega_1 & 0 & \omega_3 & -\omega_2 \\ \omega_2 & -\omega_3 & 0 & \omega_1 \\ \omega_3 & \omega_2 & -\omega_1 & 0 \end{bmatrix}$$

Quaternions themselves are great to be employed in simulations and computations but, from an human perspective, they don't describe an object's attitude as well and intuitive as Euler's angles do.

For this reason, a quaternion to Euler's angles transformation is reported as follow:

$$\begin{bmatrix} \phi \\ \theta \\ \psi \end{bmatrix} = \begin{bmatrix} atan2(2(q_0q_1 + q_2q_3), 1 - 2(q_1^2 + q_2^2)) \\ asin(2(q_0q_2 - q_3q_1)) \\ atan2(2(q_0q_3 + q_1q_2), 1 - 2(q_2^2 + q_3^2)) \end{bmatrix}$$

Using the equations (3.1) and (3.4), the base-satellite's dynamics and kinematics can be described by block diagram.

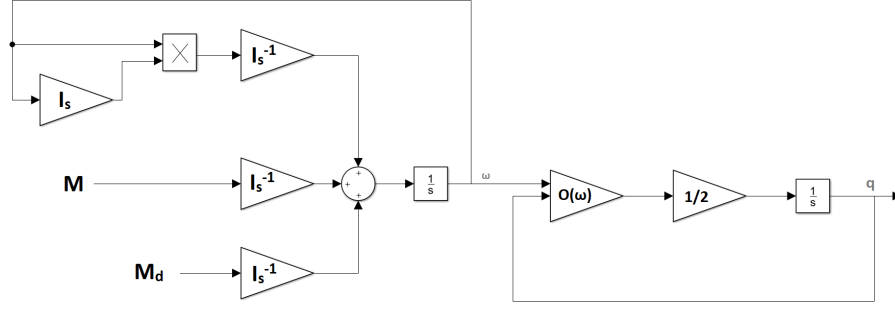


Figure 3.3: Base-Satellite dynamics and kinematics Block Diagram

3.2 Reaction Wheels Dynamic Model

The base-satellite is equipped with reaction wheels (RWs) in pyramidal configuration with a skew angle β . Such configuration provides redundancy in case of faults.

While rotating, each reaction wheel (RW) produces an angular momentum acting along the z axis in the RW reference frame.

As shown in Fig. 3.4, the wheels act in different directions with respect to the base-satellite reference frame; to express such actions, as angular momentum or torques, in the base-satellite frame J_0 , a matrix $Z \in \mathbb{R}^{3 \times 4}$ (3.5) is employed to perform the transformation and express the wheels actions in the base-satellite frame.

$$Z = \begin{bmatrix} \sin(\beta) & 0 & -\sin(\beta) & 0 \\ 0 & \sin(\beta) & 0 & -\sin(\beta) \\ \cos(\beta) & \cos(\beta) & \cos(\beta) & \cos(\beta) \end{bmatrix} \quad (3.5)$$

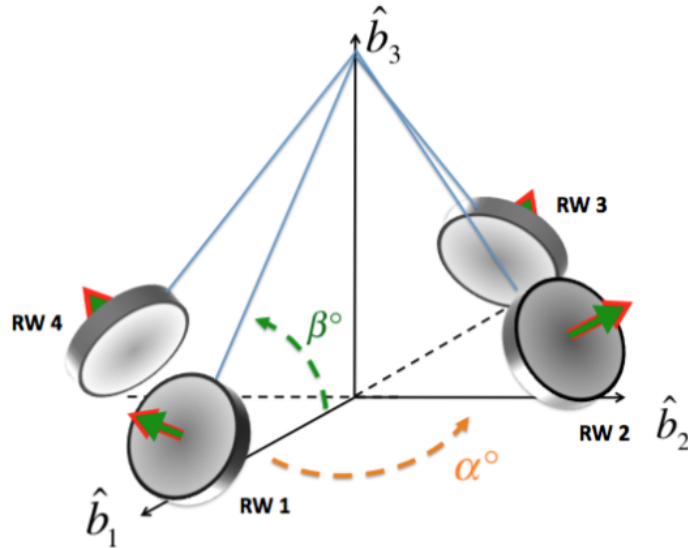


Figure 3.4: Reaction wheels pyramidal configuration. Figure from [26]

As explained in [26] the equations ruling the RWs dynamics are here reported.

The torque acting on the satellite body τ_{sat} is a contribution of the angular velocity of the satellite ω_{sat} and RWs angular momentum and torques: h_{rw}^w , τ_w^w , respectively.

$$\tau_{sat} = Z\tau_w^w + \omega_{sat} \times Zh_{rw}^w \quad (3.6)$$

The relation linking τ_{rw} with the command torque τ_c is show below:

$$\tau_{rw} = pinv(Z)(-\tau_c - \omega_{sat} \times Zh_{rw}^w) \quad (3.7)$$

Given the definition of the angular momentum

$$h_{rw} = \int \tau_w^w dt \quad (3.8)$$

The RWs, in this case, from a control system point of view are a negative, unitary gain because of the action-reaction principle.

A block diagram, using (3.5), (3.8) and (3.7) can be derived and reported below:

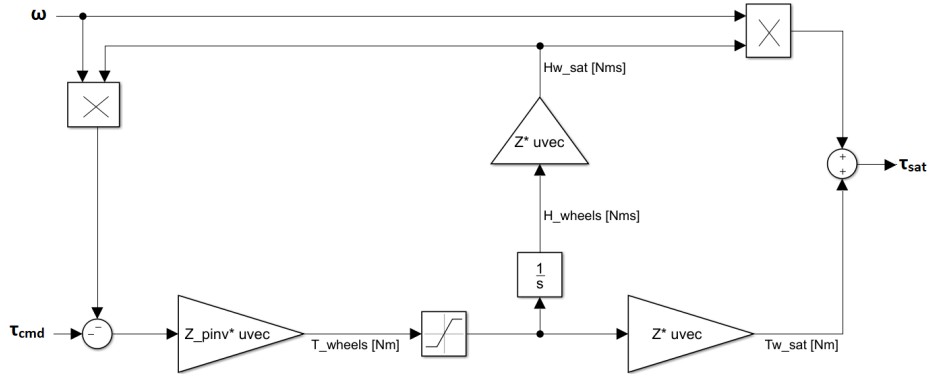


Figure 3.5: Reaction Wheel Block Diagram

The complete base-satellite model is shown in Fig.3.6. Clearly, this model is torque-driven.



Figure 3.6: Base-satellite model block diagram

3.3 Base-Satellite Sliding Mode Attitude Controller

The sliding surface s_s is designed as:

$$s_s = \omega_e + kq_e \quad (3.9)$$

Where $\omega_e = \omega_r - \omega$ is the angular velocity error while q_e is the vectorial part of the error quaternion. The error quaternion is defined as:

$$q_e = q \otimes q_r^{-1} \quad (3.10)$$

Where q_r is the reference quaternion and \otimes indicates the quaternion product [23] defined as:

$$q \otimes g = (q_0g_0 - qg) + (q_0g + g_0q + q \times g) \quad (3.11)$$

For the case of the unit quaternions, like this one, the following relation is valid:

$$q^{-1} = q^* = [q_0 \ -q_{123}] \quad (3.12)$$

An alternative representation of the quaternion error is expressed in the matrix form:

$$\begin{bmatrix} q_{e0} \\ q_{e1} \\ q_{e2} \\ q_{e3} \end{bmatrix} = \begin{bmatrix} q_{r0} & q_{r1} & q_{r2} & q_{r3} \\ -q_{r1} & q_{r0} & q_{r3} & -q_{r2} \\ -q_{r2} & -q_{r3} & q_{r0} & q_{r1} \\ q_{r3} & q_{r2} & -q_{r1} & q_{r0} \end{bmatrix} \begin{bmatrix} q_0 \\ q_1 \\ q_2 \\ q_3 \end{bmatrix} \quad (3.13)$$

Computing the surface derivation \dot{s}_s and imposing it as zero, the following result is obtained:

$$\dot{s}_s = \dot{\omega}_e + k\dot{q}_e = \dot{\omega}_r - \dot{\omega} + \frac{1}{2}k(q_{e0}\omega_e + q_e \times (\omega_r + \omega)) = 0 \quad (3.14)$$

To achieve a control law, the plant's dynamic model, has to be employed.

$$\begin{cases} \dot{\omega}_r - \dot{\omega} + \frac{1}{2}k(q_{e0}\omega_e + q_e \times (\omega_r + \omega)) = 0 \\ \dot{\omega} = -I_s^{-1}(\omega \times I_s\omega) + I_s^{-1}\tau \end{cases} \quad (3.15)$$

Thus, with few steps it's possible to express the torque's equation:

$$\tau = I_s(\dot{\omega}_r - \frac{1}{2}k(q_{e0}\omega_e + q_e \times (\omega_r + \omega))) + (\omega \times I_s\omega) \quad (3.16)$$

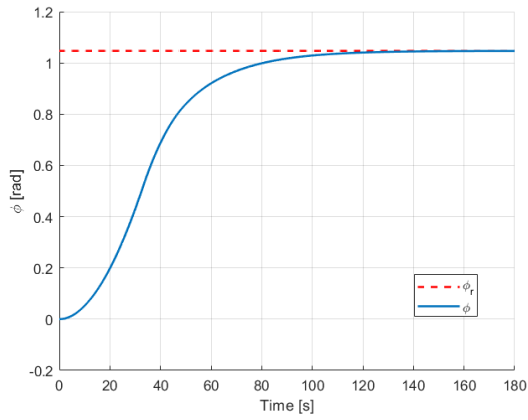
In order to make the sliding surface more attractive, an additional term is added, leading to the following control law.

$$\tau = I_s(\dot{\omega}_r - \frac{1}{2}k(q_{e0}\omega_e + q_e \times (\omega_r + \omega))) + (\omega \times I_s\omega) - cI_s \tanh(\mu s_s) \quad (3.17)$$

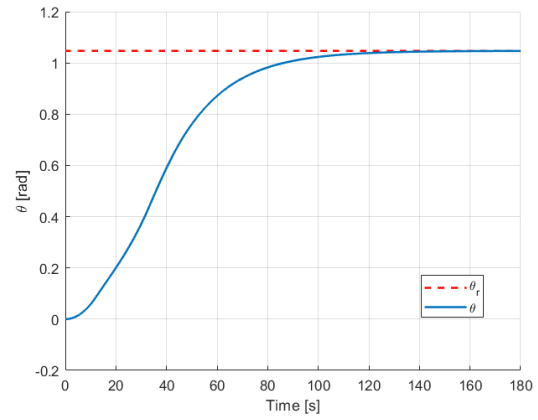
The control law (3.17) is derived by the base-satellite model alone and does not consider the reaction wheels model as actuator. To consider the negative and unitary actuator gain into the control law, the control torque has to be inverted. In this way, the system would have two negative, unitary gains in series, cancelling each others. The final control law then is shown in (3.18)

$$\tau_{cmd} = -\tau \quad (3.18)$$

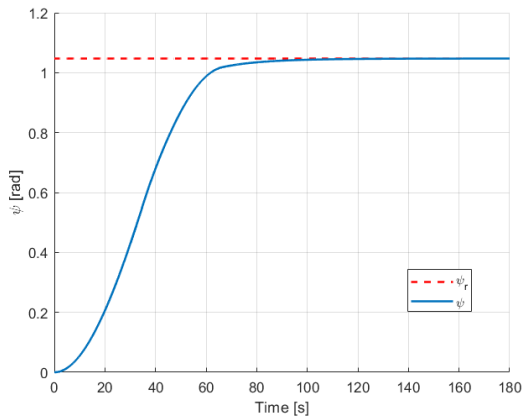
An easy maneuver is simulated in order to validate the correct behavior of the controller. The simulated maneuver consist in a $\frac{\pi}{3}$ rotation about the main axes.



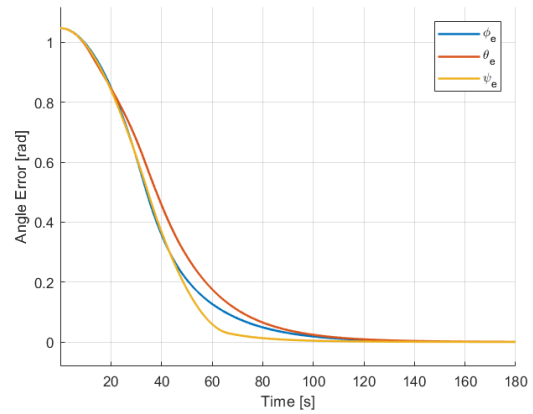
(a) ϕ tracking



(b) θ tracking



(c) ψ tracking



(d) Euler's angle tracking error

Figure 3.7: Base-satellite attitude controller performances

The base-satellite starts from the initial attitude $\Phi(t = 0) = [0 \ 0 \ 0]$ rad and reach the desired final pose $\Phi(t = t_{END}) = [\frac{\pi}{3} \ \frac{\pi}{3} \ \frac{\pi}{3}]$ rad in around two minutes. This simulation has been made with the parameters described in Chapter 6.

Chapter 4

Manipulator Model and Control

This chapter explains how the manipulator is modeled and controlled. Since in orbital manipulators the joints are prevalent revolute ones [27], all the manipulator's joints are of such type. The manipulator considered is composed by two links, and three revolute joints placed in a double pendulum-like configuration. A base-link connects the upper part of the base-satellite to the first revolute joint.

The controller employed here is, again, a Sliding Mode Controller in the Joint's Space. That means that the controller acts on the joint's angles instead of the EndEffector's position.

4.1 3 DoF Manipulator Model

The manipulator considered is a 3DoF one with revolute joints only and two links as Fig. 4.1 shows.

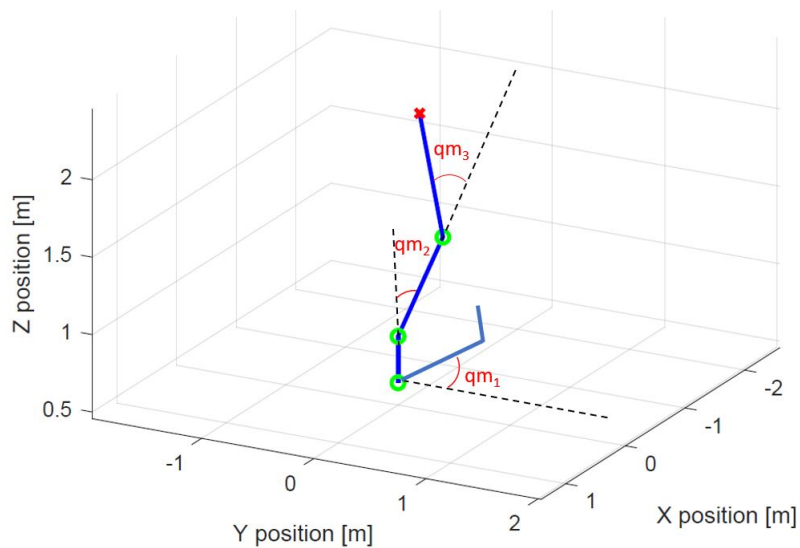


Figure 4.1: 3 DoF manipulator with 3 revolute joints and two links

The following notation is adopted:

- L : length of the links
- m : mass of the links
- qm_i : i -th revolute joint angle with respect to the i -th joint RF J_i

No presence of friction or dissipation are assumed and, since this manipulator is intended to operate in a micro-gravity environment, gravity is not taken into account. Also, the center of mass of each link is supposed to be in the very centre of each link.

Given the structure of the manipulator described in Fig. 4.1, it's possible to understand that the joint 1, the one on the base acting with its torque on the z axis, is not affected by the movements of joints 2 and 3. This configuration allows to separate the model for the base revolute joint and the two link part. Thus, what follows next is the modeling of the two-link part, considered as a planar manipulator.

Using the Lagrange approach adopted in [28] and choosing $L_1 = L_2 = L$ and $m_1 = m_2 = m$, the dynamic equations derived are:

$$\tau_{23} = M_{23}(qm)\ddot{q}m_{23} + V_{23}(qm, \dot{q}m)\dot{q}m_{23} \quad (4.1)$$

where:

$$M_{23}(qm) = \begin{bmatrix} 3mL^2 + 2mL^2c_2 & mL^2c_3 + mL^2 \\ mL^2c_3 + mL^2 & mL^2 \end{bmatrix}$$

$$V_{23}(qm, \dot{q}m) = \begin{bmatrix} mL^2s_2\dot{q}m_3 & mL^2s_2\dot{q}m_2 - mL^2s_2\dot{q}m_3 \\ mL^2s_2\dot{q}m_2 & 0 \end{bmatrix}$$

$$\tau_{23} = \begin{bmatrix} \tau_2 \\ \tau_3 \end{bmatrix}$$

Since the manipulator is intended to be controlled acting on the joints' torques, the equation (4.1) has to be inverted, producing (4.2)

$$\ddot{q}m_{23} = [\tau_{23} - V_{23}(qm, \dot{q}m)\dot{q}m_{23}]M_{23}(qm)^{-1} \quad (4.2)$$

The base joint acts in a different direction than the other two, so the reactions of the other manipulator structure don't affect the dynamics of the base joint but surely change the moment of inertia with respect of the z axis. Modeling the base joint is a simple SISO system. The equation representing this part is

$$\tau_1 = J_z(qm)\ddot{q}m_1 \quad (4.3)$$

Where $J_z(qm) = m(Lc_2)^2 + m(Lc_{23})^2$ is the inertia moment referred to the z axis. Also in this case the control input is a torque then, the equation has to be inverted:

$$\ddot{m}_1 = J_z(qm)^{-1} \tau_1 \quad (4.4)$$

Merging the two parts the entire model is obtained. The new matrices are:

$$M(qm) = \begin{bmatrix} m(Lc_2)^2 + m(Lc_{23})^2 & 0 & 0 \\ 3mL^2 + 2mL^2c_2 & mL^2c_3 + mL^2 & 0 \\ mL^2c_3 + mL^2 & mL^2 & 0 \end{bmatrix} \quad (4.5)$$

$$V(qm, \dot{q}m) = \begin{bmatrix} 0 & 0 & 0 \\ mL^2s_2\dot{q}m_3 & mL^2s_2\dot{q}m_2 - mL^2s_2\dot{q}m_3 & 0 \\ mL^2s_2\dot{q}m_2 & 0 & 0 \end{bmatrix} \quad (4.6)$$

$$\tau = \begin{bmatrix} \tau_1 \\ \tau_2 \\ \tau_3 \end{bmatrix} \quad (4.7)$$

Of course, the final equations are:

$$\tau = M(qm)\ddot{q}m + V(qm, \dot{q}m)\dot{q}m \quad (4.8)$$

Also the manipulator is considered to be torque-driven. Hence:

$$\ddot{q}m = M(qm)^{-1}\tau - M(qm)^{-1}V(qm, \dot{q}m)\dot{q}m \quad (4.9)$$

Another notable aspect in robotic is the Direct Kinematics defined as the function $\mathcal{DK}(qm)$ starting from the joint space and computing the End Effector's position and orientation in the real space.

$$\mathcal{DK} : qm \rightarrow EE_p \quad (4.10)$$

In this thesis the manipulator has no wrist, so the position is sufficient to describe the End Effector's pose.

In this case, the Forward Kinematics with respect to the base-satellite's RF J_0 , is reported in (4.11)

$$\begin{bmatrix} x_{EE} \\ y_{EE} \\ z_{EE} \end{bmatrix} = \begin{bmatrix} L \cos(qm_1) [\cos(qm_2) + \cos(qm_2 + qm_3)] \\ L \sin(qm_1) [\cos(qm_2) + \cos(qm_2 + qm_3)] \\ L [\sin(qm_2) + \sin(qm_2 + qm_3)] + L_b + h/2 \end{bmatrix} \quad (4.11)$$

The manipulator is intended to be mounted on top of the base-satellite described in the previous chapter; this fact affects the range of the joints' angles, thus the working space, in order to avoid collisions. The working space is defined as the subspace reachable by the manipulator's End Effector (EE). In this particular case, the manipulator's joints' angle are limited to the following ranges:

$$\begin{aligned} 0 &\leq q_{m1} < 2\pi \\ -\frac{\pi}{2} &\leq q_{m2} \leq \frac{\pi}{2} \\ -\frac{\pi}{2} &\leq q_{m3} \leq \frac{\pi}{2} \end{aligned}$$

Given those angular constraints, the manipulator's working space is shown in Fig. 4.2

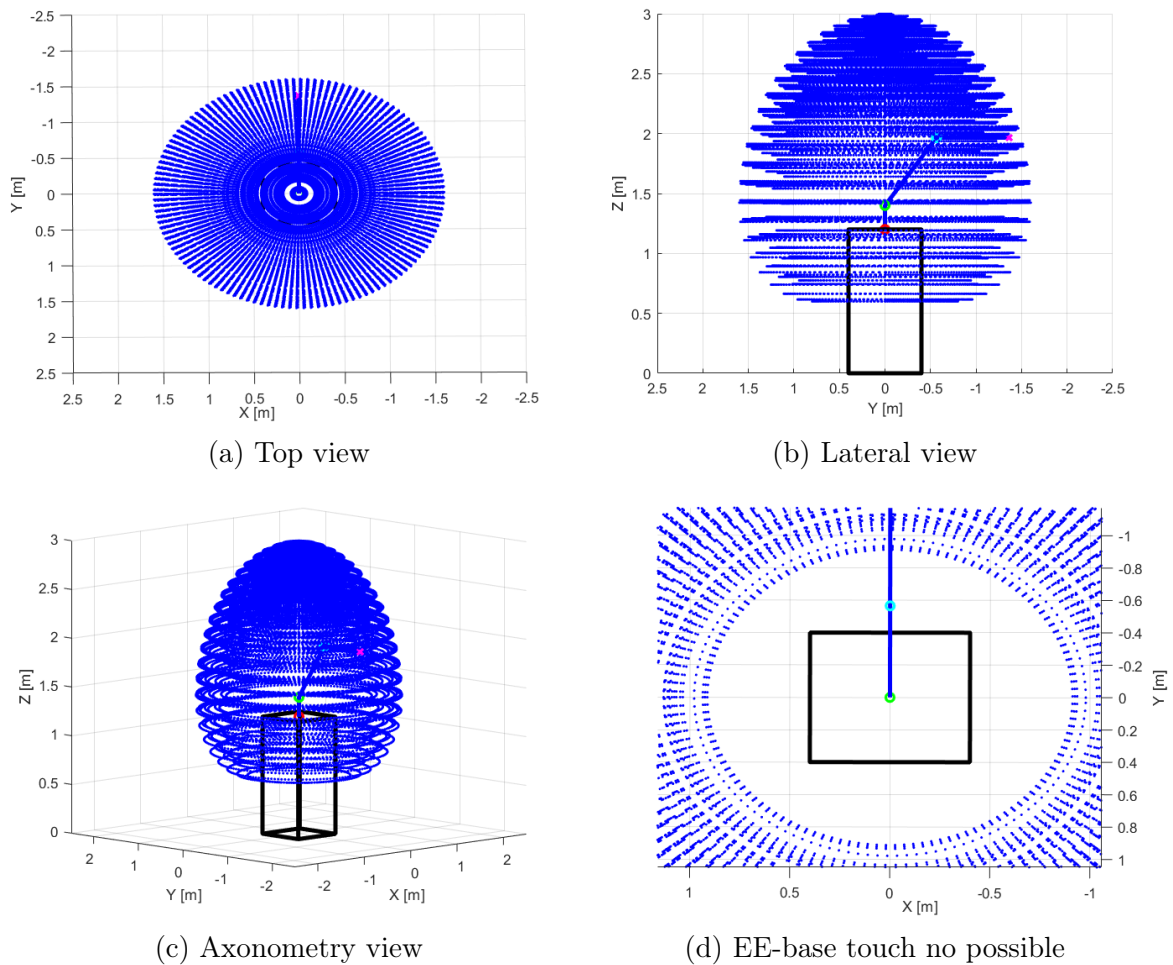


Figure 4.2: Manipulator working space

The figures in 4.2 show the working space given the constraints and considering the parameters used in the simulations (i.e. links; length $L = 0.8 \text{ m}$)

It's possible to see that the End Effector can't reach the base-satellite's body despite covering the surrounding of its upper part.

4.2 Manipulator Sliding Mode Control

The controller design is very similar to the ones explained for the base-satellite in Section 3.3. Inverting the equation the manipulator dynamics, considering the input torque, is:

$$\ddot{m} = M^{-1}\tau - M^{-1}V\dot{m} \quad (4.12)$$

In this case, the sliding surface s_m is defined as

$$s_m = \ddot{m}_e + k_1\dot{m}_e + k_2qm_e = 0 \quad (4.13)$$

Considering $\dot{m}_r = 0$ rad/s and substituting the joints accelerations given by the dynamic equation:

$$s_m = M^{-1}\tau - M^{-1}V\dot{m} + k_1\dot{m} + k_2qm_e = 0 \quad (4.14)$$

Highlighting the torque and adding an additional term to make sliding surface s_m more attractive:

$$\tau_{cmd} = V\dot{m} + M(k_2qm_e - k_1\dot{m}) + ctanh(s_m) \quad (4.15)$$

Apart from control the manipulator, this controller has to make the manipulator reach its reference state in the smoothest way possible. This is because, with a smoother tracking, it's more likely to avoid reactions persisting for larger time windows on the base-satellite. From the performances point of view, this mean to design the manipulator system to be overdamped. The drawback with overdamped system is a long reaching time. A trade-off may be the design of a critically damped system, such system should have a shorter rising time compared to the overdamped one and no overshoots.

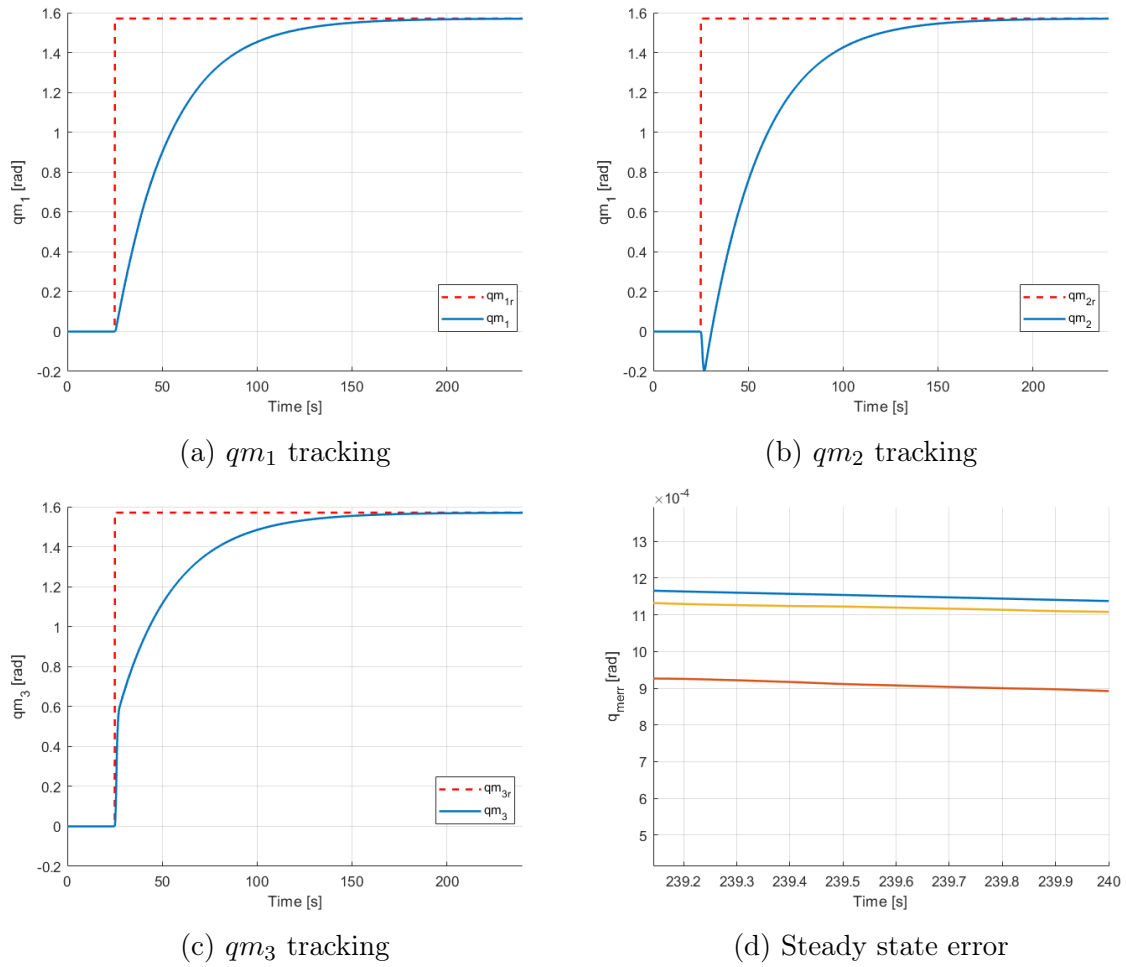


Figure 4.3: Manipulator's SMC performances

Fig. 4.3 shows that the reaching time is quite large, around 200 s but, once steady state is reached, the tracking error is practically null and, most importantly, there is no overshoot.

Chapter 5

Multi-body Plant Dynamics Model

In this chapter the entire multi-body is considered and modeled through the equations of motion derived from the Lagrange approach, an alternative to the Newton approach.

An advantage of the Lagrange approach is that such methodology allows to describe the system through the kinetic and potential energies, which are additive scalar quantities and can be seen as a state function of a multi-body system. The Lagrangian approach derives in part from the Principle of Least Action, which states that a physical system tends to minimize its kinetic energy. From the mathematical point of view, it states that the action of the system, defined as \mathcal{S} in (5.1), is minimized.

$$\mathcal{S} = \int_{t_1}^{t_2} \mathcal{L}(q, \dot{q}, t) dt \quad (5.1)$$

The inner item of the Lagrange approach is the Lagrangian \mathcal{L} , a mathematical function which summarizes the dynamic of the systems using its energies.

$$\mathcal{L}(q, \dot{q}, t) = \mathcal{K}(q, \dot{q}) - \mathcal{P}(q) \quad (5.2)$$

The terms q and \dot{q} indicate the generalized coordinates and generalized velocities respectively and they are chosen to actually represent the position and velocity of each body in the entire system.

The Lagrange equations are reported in (5.3), where ξ indicates the generalized forces.

$$\frac{d}{dt} \left(\frac{\partial \mathcal{L}}{\partial \dot{q}} \right) - \frac{\partial \mathcal{L}}{\partial q} = \xi \quad (5.3)$$

The system is implemented using SPART, a MATLAB Toolbox [29]. SPART allows different descriptions of multi-body systems, this thesis employed the Denavit-Hartenberg description.

5.1 Reference Frames

First step required to build a model is setting the reference frames (RFs). Some reference frames have been already introduced in the previous chapters and here are recalled again for better understanding.

Three types of reference frames are employed to describe the kinematics of this system: an inertial one J , joint-fixed ones J_i and link-fixed ones \mathcal{L}_i .

Each manipulator joint has its reference frames oriented as suggested by the Denavit-Hartenberg convention [30]. The z-axis is directed along the joint's rotation axis k_i , the x-axis is pointing the next joint and the y-axis is obtained using the right hand rule. The manipulator links are considered as an homogeneous one, the CoM of one link is located in the middle of it, making the discussion easier. As suggested in [27], the joint-fixed reference frames \mathcal{L}_i is oriented the same way the joint-fixed J_{i+1} is. An example is shown in Fig. 5.1.

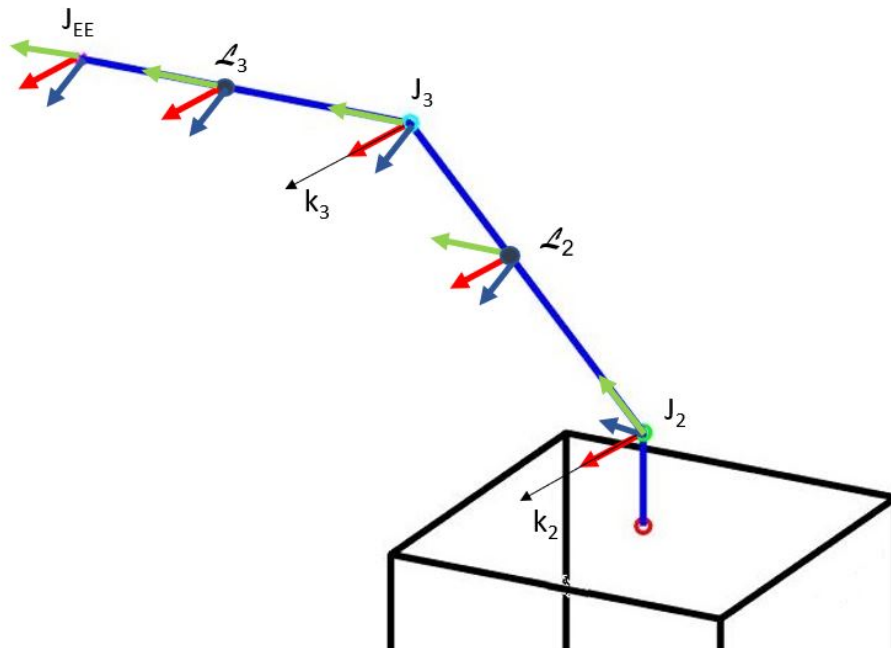


Figure 5.1: Examples of J_i (Joint RFs) and \mathcal{L}_i (CoMs RFs)

A special case is the base-satellite, which can be considered as link 0, where the joint's RF is equivalent to CoM's RF, then $J_0 = \mathcal{L}_0$.

5.2 Equations of Motion

To well describe the multi-body system, the equations of motion are employed. Such equations can be computed using the Lagrange approach.

Due the small presence of micro-gravity in orbit the potential energy is considered null, thus the total energy of the system is just the kinetic one, \mathcal{K} defined in (5.4).

$$\mathcal{L} = \mathcal{K} = \frac{1}{2} \sum_{i=1}^n ({}^J\omega_i^T {}^J I_i {}^J\omega_i + m_i {}^J\dot{r}_i^T {}^J\dot{r}_i) \quad (5.4)$$

Where r_i is the distance of the CoM_i from the inertial reference frame, ω_i are the angular velocities of both manipulator's joints and base-satellite, expressed in the inertial reference frames as well.

Writing (5.4) in matrix form is possible to highlight the different terms present in the inertia matrices of the system.

$$\mathcal{K} = \frac{1}{2} [{}^J\dot{x}_0^T \dot{q}^T] \begin{bmatrix} H_0 & H_{0m} \\ H_{0m}^T & H_m \end{bmatrix} \begin{bmatrix} {}^J\dot{x}_0 \\ \dot{q} \end{bmatrix} \quad (5.5)$$

Where ${}^J\dot{x}_0$ collects both the linear and angular velocities of the base-satellite expressed in the inertial RF J, so ${}^J\dot{x}_0 = [{}^J\dot{v}_0^T {}^J\dot{\omega}_0^T]^T$.

In this case, where the manipulator is composed of three links, the matrices and their dimensions are $H_0 \in \mathbb{R}^{6,6}$ is the base-satellite inertia matrix, $H_m \in \mathbb{R}^{3,3}$ is the manipulator inertia matrix and $H_{0m} \in \mathbb{R}^{6,3}$ is the matrix considering the coupling effects. The dimension of such matrices depends by the number of links in the manipulator.

All the matrices listed before are well described in [27] and here reported.

Starting from the base-satellite matrix H_0 .

$$H_0 = \begin{bmatrix} m_{tot} I_{3,3} & -m_{tot} {}^J r_{0C}^\times \\ m_{tot} {}^J r_{0C}^\times & H_s \end{bmatrix} \quad (5.6)$$

Where m_{tot} indicates the total mass of the system.

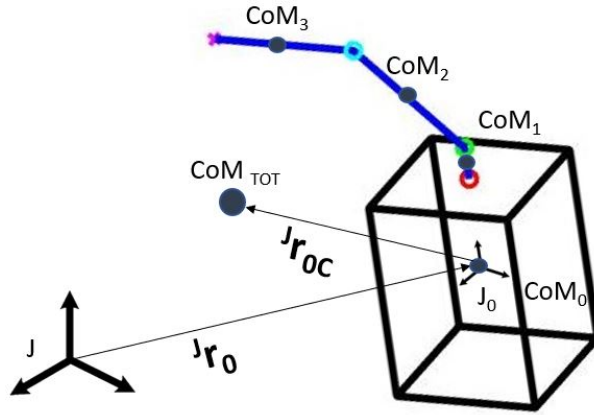
$$m_{tot} = m_0 + \sum_{i=1}^3 m_i \quad (5.7)$$

Since the manipulator can change position, the position of the CoM of the system changes. In order to geometrically represent the system's CoM, ${}^J r_{0C}$ indicates the vector starting from the base-satellite RF J_0 pointing the system's CoM.

$${}^J r_{0C} = \frac{1}{m_{tot}} \sum_{i=1}^3 m_i {}^J r_{0i} \quad (5.8)$$

The term ${}^J r_{0C}^\times$ means that the vector is written in the skew-symmetric matrix form as show in (5.9).

$${}^J r_{0C}^\times = \begin{bmatrix} 0 & -J r_{0C_z} & J r_{0C_y} \\ J r_{0C_z} & 0 & -J r_{0C_x} \\ -J r_{0C_y} & J r_{0C_x} & 0 \end{bmatrix} \quad (5.9)$$

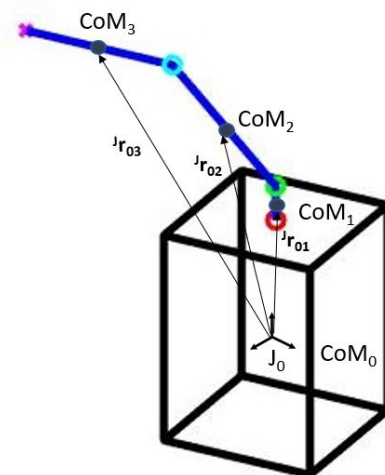

 Figure 5.2: ${}^J r_{0C}$ representation

H_S considers the moments of inertia with respect to the base-satellite RF J_0 , taking into account the manipulator's links, and expressed in the inertial RF J . Basically H_S express the parallel axis theorem for the moments of inertia of all the system's components.

$$H_S = \sum_{i=1}^3 ({}^J I_i - m_i {}^J r_{0i}^\times {}^J r_{0i}^\times) + {}^J I_0 \quad (5.10)$$

${}^J r_{0i}^\times$ is the vector starting from the base-satellite RF J_0 and pointing the i -th link's CoM, expressed as shown in (5.9).

Fig 5.3 shows the geometrical meaning of the vectors used in the previous equations.


 Figure 5.3: ${}^J r_{0i}$ representations

Since the moments of inertia of the elements composing the multi-body system are expressed in the i -th link RF \mathcal{L}_i , some transformations have to be employed, using the direction-cosine matrices (DCMs) ${}^J R_{\mathcal{L}_i}$, in order to describe such moments of inertia in the inertia RF J .

$${}^J I_i = {}^J R_{\mathcal{L}_i} {}^{\mathcal{L}_i} I_i {}^J R_{\mathcal{L}_i}^T \quad (5.11)$$

A generic ${}^J R_{\mathcal{L}_i}$ represent the rotation between the RF \mathcal{L}_i and \mathcal{L}_{i-1} . This matrices can be obtained exploiting the Denavit-Hartenberg convection [30] and can be multiplied one after the other to described a sequence of rotations.

Matrix H_{0m} express the dynamic coupling terms between the manipulator and the base-satellite in terms of kinetic energy.

$$H_{0m} = \begin{bmatrix} \sum_{i=1}^3 (m_i {}^J J_{T_i}) \\ \sum_{i=1}^3 ({}^J I_i {}^J J_{R_i} + m_i {}^J r_{0i}^\times {}^J J_{T_i}) \end{bmatrix} \quad (5.12)$$

Where ${}^J J_{T_i}$ and ${}^J J_{R_i}$ represent the Jacobian linear velocity of the i -th link's CoM and the Jacobian angular velocities of i -th link respectively.

$${}^J J_{T_i} = [{}^J k_1^\times ({}^J r_i - {}^J p_1) \dots {}^J k_i^\times ({}^J r_i - {}^J p_i) 0_{3,2}], \quad \forall (1 \leq i \leq 3) \quad (5.13)$$

$${}^J J_{R_i} = [{}^J k_1 \dots {}^J k_i 0_{3,2}], \quad \forall (1 \leq i \leq 3) \quad (5.14)$$

Regarding the manipulator inertia matrix H_m , it contains the kinetic energy contribution, in both rotational and linear means, when considering just the manipulator, as reported in Eq. (5.15).

$$H_m = \sum_{i=1}^3 ({}^J R_i^T {}^J I_i {}^J R_i + m_i {}^J J_{T_i}^T {}^J J_{T_i}) \quad (5.15)$$

Once the matrices have been defined, it's possible to move them into the Lagrange equations. In this case it's convenient to classify the Lagrange equations in two parts: one describing the base-satellite (5.16) and another describing the manipulator (5.17).

$$\frac{\partial}{\partial t} \left(\frac{\partial \mathcal{K}}{\partial \dot{x}_0} \right) - \frac{\partial \mathcal{K}}{\partial x_0} = \begin{bmatrix} 0_{3,1} \\ \tau_{sat} \end{bmatrix} \quad (5.16)$$

$$\frac{\partial}{\partial t} \left(\frac{\partial \mathcal{K}}{\partial \dot{q}_m} \right) - \frac{\partial \mathcal{K}}{\partial q_m} = \tau_m \quad (5.17)$$

Solving the Lagrangian leads the equations of motion, shown in (5.18)

$$\begin{bmatrix} H_0 & H_{0m} \\ H_{0m}^T & H_m \end{bmatrix} \begin{bmatrix} \ddot{x}_0 \\ \ddot{q}_m \end{bmatrix} + \begin{bmatrix} C_0 & C_{0m} \\ C_{0m}^T & C_m \end{bmatrix} \begin{bmatrix} \dot{x}_0 \\ \dot{q}_m \end{bmatrix} = \begin{bmatrix} 0_{3,1} \\ \tau_{sat} \\ \tau_m \end{bmatrix} \quad (5.18)$$

There are some null terms in the generalized forces in (5.16) and (5.18) because those terms represent the linear external forces, which are zeros since the base satellite is considered to be equipped with reaction wheels only (i.e. no thrusters).

As described in the previous chapters, the system is torque controlled; (5.18) has to be inverted:

$$\begin{bmatrix} \ddot{x}_0 \\ \ddot{q}_m \end{bmatrix} = \begin{bmatrix} H_0 & H_{0m} \\ H_{0m}^T & H_m \end{bmatrix}^{-1} \begin{bmatrix} 0_{3,1} \\ \tau_{sat} \\ \tau_m \end{bmatrix} - \begin{bmatrix} H_0 & H_{0m} \\ H_{0m}^T & H_m \end{bmatrix}^{-1} \begin{bmatrix} C_0 & C_{0m} \\ C_{0m}^T & C_m \end{bmatrix} \begin{bmatrix} \dot{x}_0 \\ \dot{q}_m \end{bmatrix} \quad (5.19)$$

5.3 Manipulator Reaction on the Base-Satellite

Since the manipulator and the base-satellite are connected by mechanical means, an action from a component affect the other ones and vice versa. Since the main goal of this work of thesis is focused on the attitude of the base-satellite, the manipulator's reactions on the base-satellite are considered only. In order to quantify such reactions, it possible to exploit the equations (5.18). Considering just the torques acting on the base-satellite:

$$\begin{bmatrix} F_s \\ \tau_s \end{bmatrix} = H_0 \ddot{x}_0 + H_{0m} \ddot{q}_m + C_0 \dot{x}_0 + C_{0m} \dot{q}_m \quad (5.20)$$

and taking into account just the terms due to the manipulators:

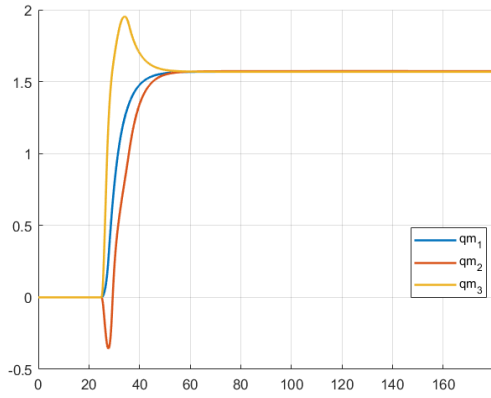
$$\begin{bmatrix} F_s \\ \tau_s \end{bmatrix}_m = H_{0m} \ddot{q}_m + C_{0m} \dot{q}_m \quad (5.21)$$

These are the reactions, by both linear forces and torques means, that the moving manipulator produces on the base-satellite. The linear forces act on the base-satellite affecting its displacement in space but since the free-floating manipulator system is considered on the attitude aspect only, that is not a concern in this thesis. Also, those linear reactions can be considered as disturbances in a orbital controller.

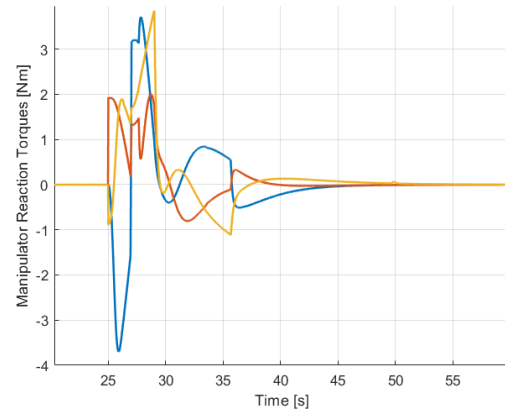
The reaction torques then, affect the satellite's attitude. Recalling (5.21) and (3.1) its possible to realize that $\tau_s|_m$ can be embedded in M_d .

As (5.21) proves, such reactions depend by the joint's angles acceleration \ddot{q}_m and velocities \dot{q}_m . Thus, (5.21) suggests that to avoid significant disturbances on the base-satellite's attitude, the manipulator has to be subjected to low joint's angles accelerations. As suggested in Section 4.2, the manipulator is designed to avoid overshoots in order to limit the action time of the manipulator's reactions.

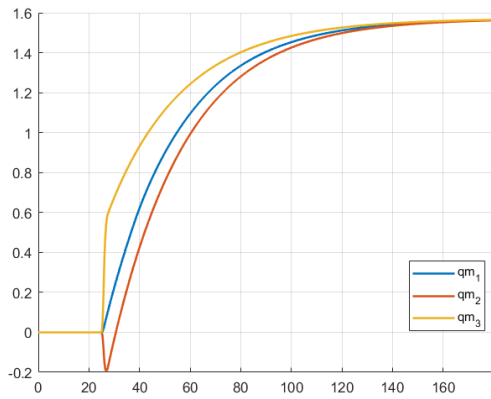
Using the equations of motion (5.19), it's possible to simulate the manipulator's reactions on the base-satellite in the case where the manipulator system is underdamped and critically damped. In Fig. 5.4, just the reaction torques $\tau_s|_m$ are reported.



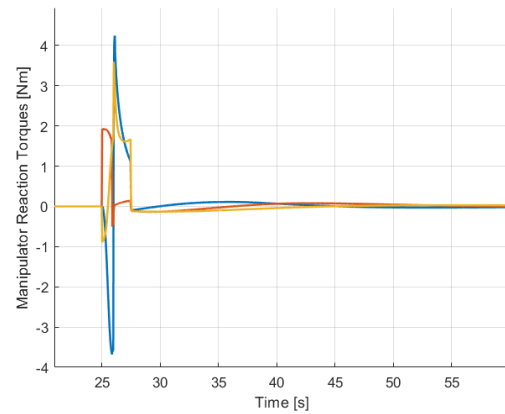
(a) Underdamped behavior



(b) Underdamped behavior's reactions



(c) Damped behavior



(d) Damped behavior's reactions

Figure 5.4: Reactions magnitude and period of action

These plots confirm and justify the smooth, slow performances of the manipulator in order to reduce the reaction time window, thus reducing their effects on the base-satellite's attitude.

5.4 SPART Implementation

The equations of motion shown in (5.18) and (5.19) are obtained using the MATLAB Tool SPART [29]. This tool needs the physical parameters and geometrical model of the system. It has several ways to describe the system, including the description through Denavit-Hartenberg parameters.

Considering the joint-fixed RFs J_i only, it's possible to obtain the Denavit-Hartenberg parameters. These parameters are very useful and widely used in robotics to define the homogeneous transformation between joint-fixed RFs J_i and, since the modeling tool accepts such parameters, they're very useful. As described in [30] and shown in Fig.5.5, the Denavit-Hartenberg parameters are:

- θ_i : rotation from x_{J_i} to $x_{J_{i+1}}$ about the i -th joint direction of rotation z_{J_i}
- α_i : rotation from z_{J_i} to $z_{J_{i+1}}$ about x_{J_i}
- d_i : distance from RF J_i and $x_{J_{i+1}}$ along z_{J_i}
- a_i : distance along the common normal between z_{J_i} along $z_{J_{i+1}}$

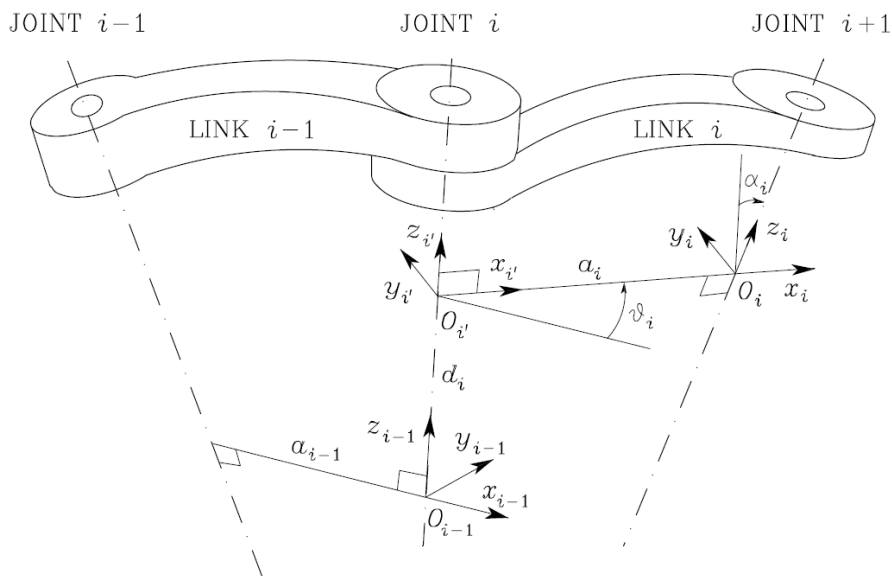


Figure 5.5: Denavit-Hartenberg parameters. Figure from *Robotics. Modelling, Planning and Control* [30]

Applying the definition of Denavit-Hartenberg parameters on the manipulator in Fig 5.6

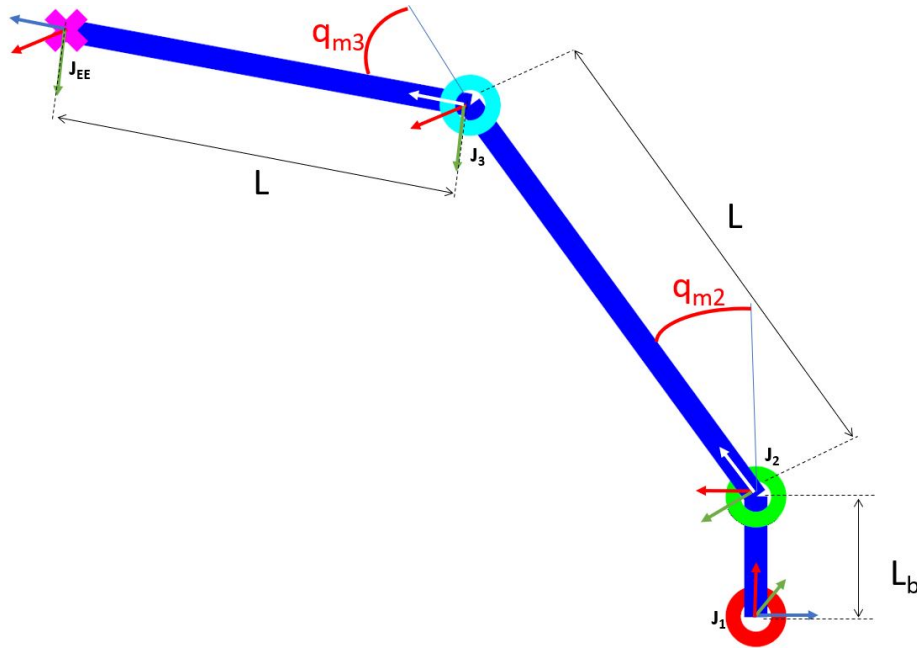


Figure 5.6: Manipulator joints and RFs

the values shown in (5.22) are obtained.

RF	θ_i	d_i	α_i	a_i
$J_1 \rightarrow J_2$	$\pi/2$	L_b	$\pi/2$	0
$J_2 \rightarrow J_3$	q_{m2}	0	0	L
$J_3 \rightarrow J_{EE}$	q_{m3}	0	0	L

(5.22)

A last homogeneous transformation 0T_1 has to be employed in order to express the position of the first joint-fixed RF J_1 with respect to the base-satellite RF J_0 .

As shown in Fig. 5.7, the first joint is located on top of the base-satellite and share the same z axis' versor, $k_{J_0} = k_{J_1}$ thus, the only rotation that may occur is the one around the k_{J_1} with the angle of rotation equal to the joint angle q_{m1} . Also, J_1 , seen from J_0 is translated right above it, with a vertical distance equal to the half of the base-satellite's height.

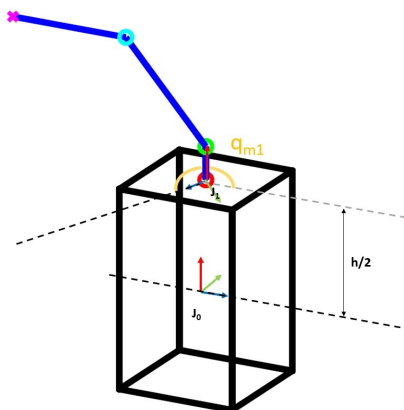


Figure 5.7

Given these last parameters and variables, the transformation matrix 0T_1 can be expressed as reported in (5.23).

$${}^0T_1 = \begin{bmatrix} \cos(q_{m1}) & -\sin(q_{m1}) & 0 & 0 \\ \sin(q_{m1}) & \cos(q_{m1}) & 0 & 0 \\ 0 & 0 & 1 & \frac{h}{2} \\ 0 & 0 & 0 & 1 \end{bmatrix} \quad (5.23)$$

Chapter 6

Simulations Results

Using MATLAB and Simulink, different simulations have been computed in order to validate the behavior of both controllers. No coupling effects are included between the two systems (base-satellite robotic arm), to have a more flexible and modular control system.

Some considerations about the system's parameters have to be made:

- The base-satellite mass's is $m_s = 200 \text{ kg}$ and its inertia matrix is $I_s = \text{diag}([50 \ 25 \ 25]) \text{kgm}^2$
- For the RWs, the Honeywell HR16 specifications are used. Refer to [31] for all the parameters.
The RW saturation torque is $\tau_{rw}|_{MAX} = 0.4 \text{ Nm}$.
The RWs are in pyramidal configurations (see Fig.3.4) with $\alpha = 90^\circ$ and skew angle $\alpha = 57.6^\circ$
- Total manipulator mass is set to be 10 % of the base-satellite's mass. $m_{arm} = 20 \text{ kg}$

Several simulations are performed considering four different scenarios:

1. The base-satellite performs a simple maneuver while the manipulator is holding a fixed position.
2. The base-satellite tracks a constant reference in order to keep its attitude while the manipulator is moving. This simulation can evaluate the base-satellite controller reactions attenuation.
3. The base-satellite perform a maneuver while also the manipulator is changing its joints' position.
4. A final simulation is performed in a Earth-Observation-like mission scenario where both the base-satellite and manipulator are moving. This simulation is performed in order to have a better understanding on how the system would behave in a more realistic scenario.

6.1 Scenario 1

In this scenario the manipulator is fixed in position $q_m = [0 \frac{\pi}{2} 0] \text{ rad}$ while the base-satellite attitude Φ performs a maneuver from $\Phi(t = 0) = [0 \ 0 \ 0] \text{ rad}$ to $\Phi(t = 240) = [\frac{\pi}{3} \ \frac{\pi}{3} \ \frac{\pi}{3}] \text{ rad}$. The quaternions tracking is shown in Fig. 6.1

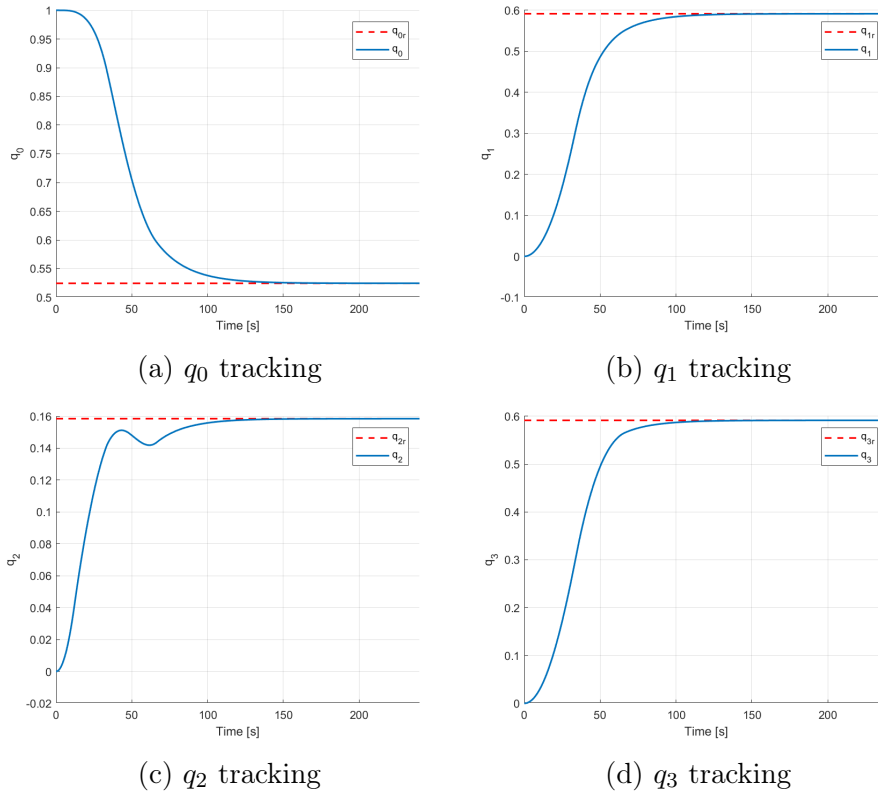


Figure 6.1: Quaternions tracking with manipulator holding a constant position

As from Fig. 6.1, the desired attitude is reached in about 120 s, with a tracking error, shown in Fig. 6.2 rapidly reaching the zero value.

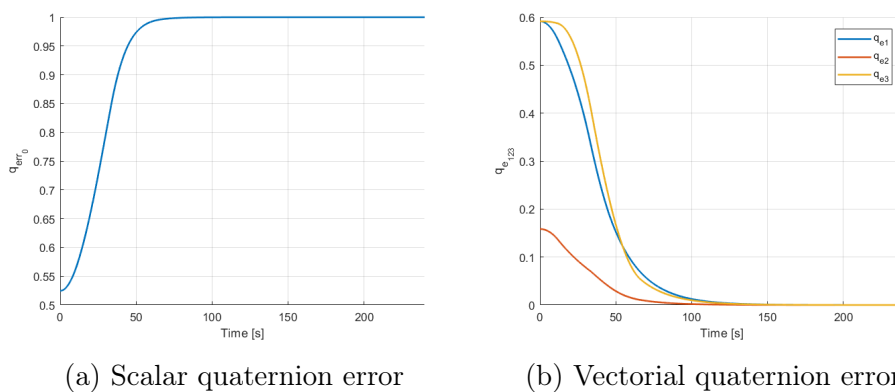


Figure 6.2: Quaternions tracking error

For a better understanding of the maneuver, the Euler's angles tracking and error are reported in Fig. 6.3

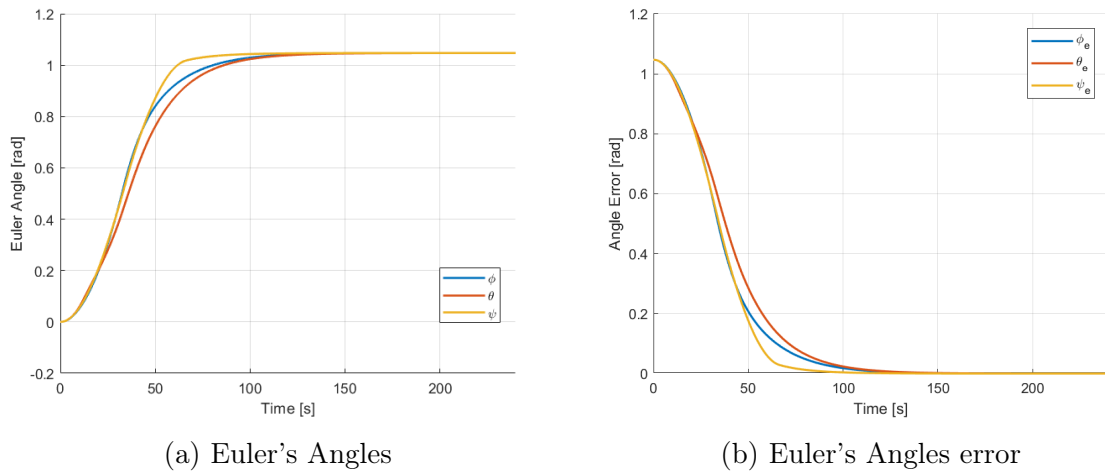


Figure 6.3: Euler's Angles

As for the quaternion behavior, Fig. 6.3 shows that the base-satellite reaches its new attitude in around 120 s.

The base-satellite input torque is reported in Fig. 6.4 To rapidly reach the desired attitude, the SMC controller applies the maximum torque at the beginning of the simulation.

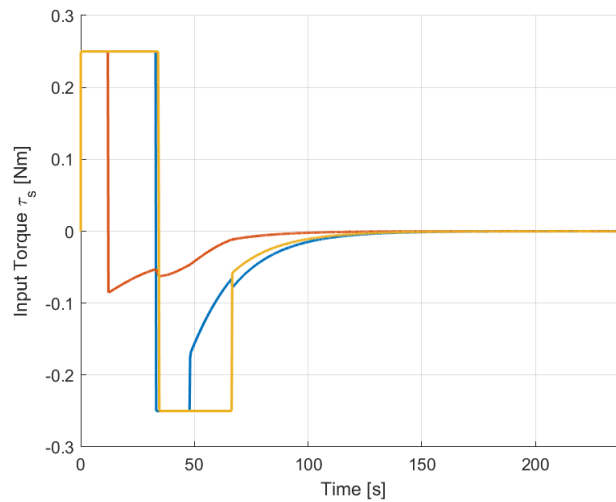


Figure 6.4: Torque input by SMC controller

6.2 Scenario 2

In the second case, the base-satellite is its desired attitude and the manipulator is moving. Hence, the base-satellite controller has to compensate the manipulator's reaction in order to keep its fixed attitude.

The manipulator start from the joint angles' pose $q_m(t = 0) = [0 \ 0 \ 0] \text{ rad}$ and track a reference set to $q_{mr} = [\frac{\pi}{2} \ \frac{\pi}{2} \ \frac{\pi}{2}] \text{ rad}$ while the base-satellite tracks a constant attitude set to $[\phi, \theta, \psi] = [0 \ 0 \ 0] \text{ rad}$. The manipulator starts to move at $t = 25 \text{ s}$.

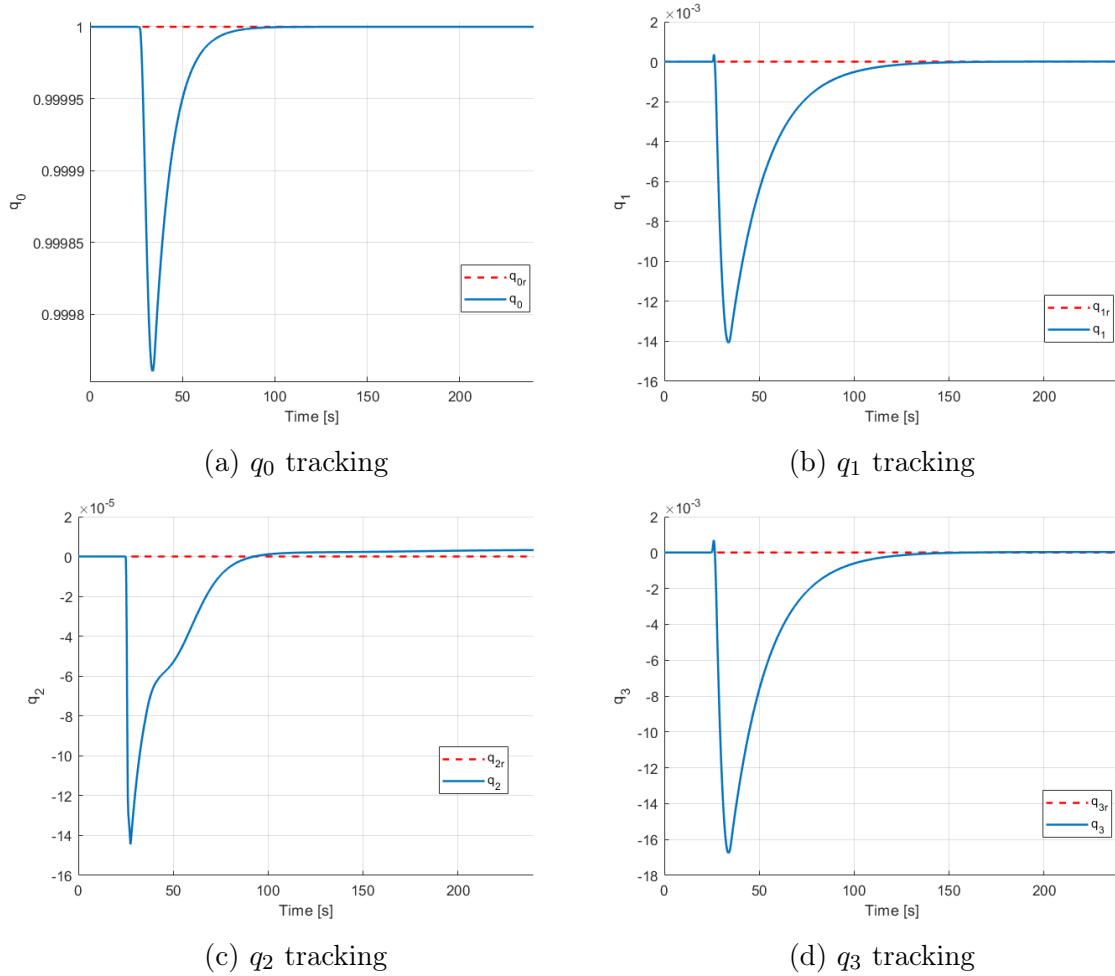


Figure 6.5: Quaternions tracking with moving manipulator and constant attitude

As Fig. 6.5 and ?? show, the error in terms of quaternion is around 10^{-3} . So the manipulator has minimum effects on the base-satellite.

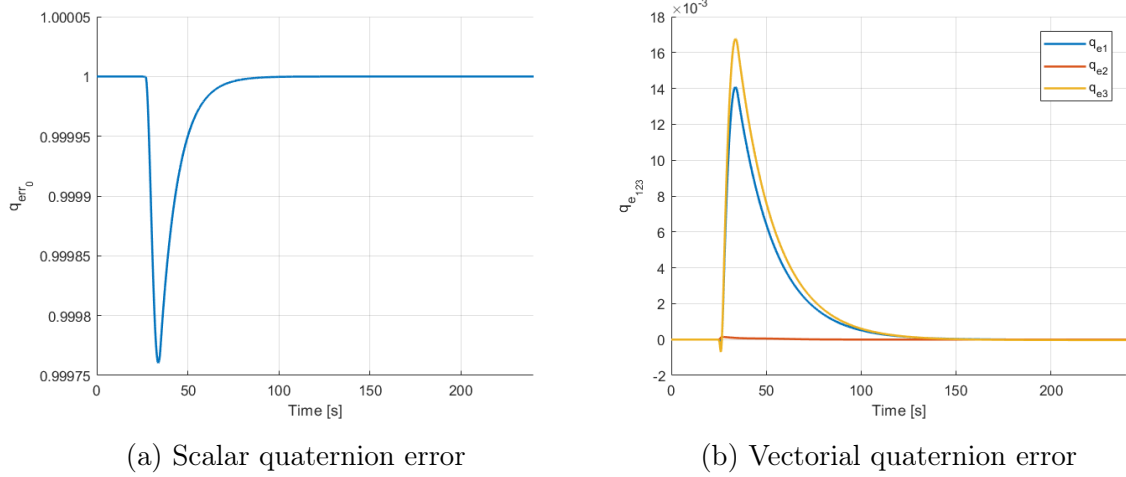


Figure 6.6: Quaternions tracking error

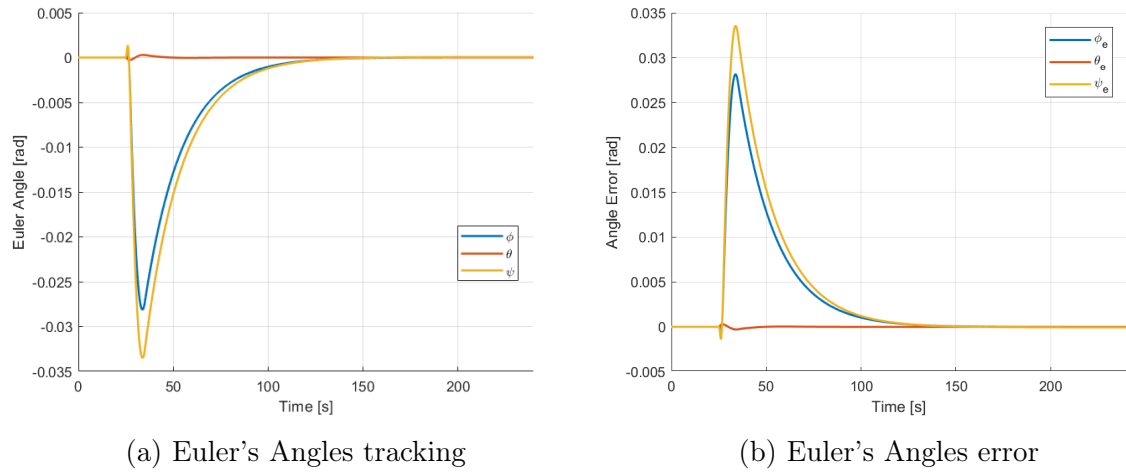


Figure 6.7: Euler's angle

As Fig. 6.7 shows, the base-satellite's attitude is changed when the manipulator starts its movements. An error peaks of about 0.03 rad is observed in Fig 6.3 due to the manipulator's movement for about 80 s .

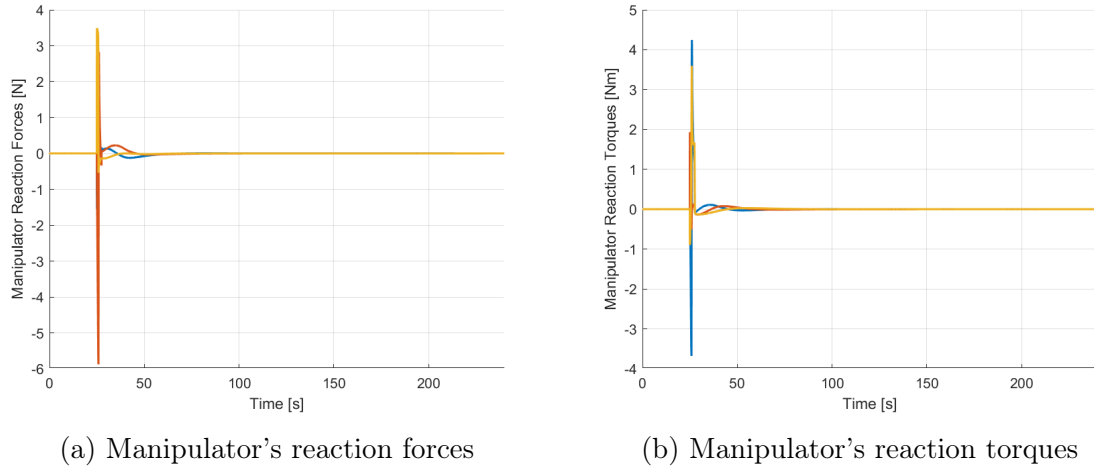


Figure 6.8: Reactions

Fig. 6.8 shows both the reaction forces and torques. Despite the magnitude of the disturbances are not negligible, the base-satellite's attitude is not heavily affected with a 0.035 rad (i.e. around 2°) error peak. The reactions that the base-satellite controller can attenuate are the reaction torques $\tau_s|_m$, the linear forces are not attenuated and lead the base-satellite's displacement to change.

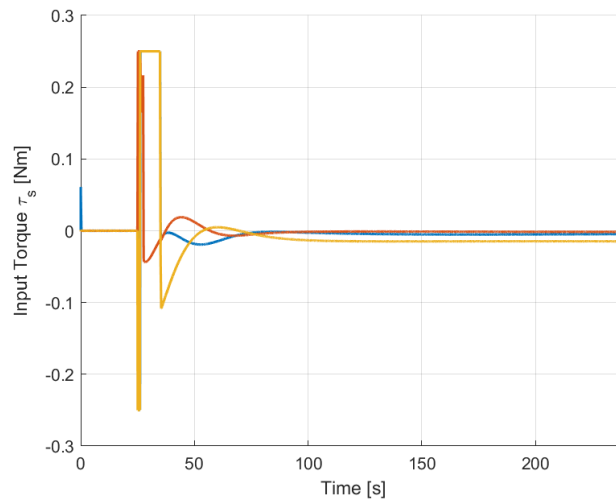


Figure 6.9: Torque input by SMC controller

However, to withstand to the manipulator's reactions, the base-satellite controller has to command the maximum torque for several seconds, as reported in Fig 6.9.

6.3 Scenario 3

This scenario basically combine Scenario 1 (Sec. 6.1) and Scenario 2 (Sec. 6.2). The purpose of this simulation scenario is understanding how the manipulator's actions affect the base-satellite's maneuver performance. Again, the base-satellite attitude Φ performs a maneuver from $\Phi(t = 0) = [0 \ 0 \ 0]$ rad to $\Phi(t = 240) = [\frac{\pi}{3} \ \frac{\pi}{3} \ \frac{\pi}{3}]$ rad while the manipulator, with initial joints' position $qm = [0 \ 0 \ 0]$ rad, tracks $qm = [\frac{\pi}{2} \ \frac{\pi}{2} \ \frac{\pi}{2}]$ rad starting from $t = 25$ s

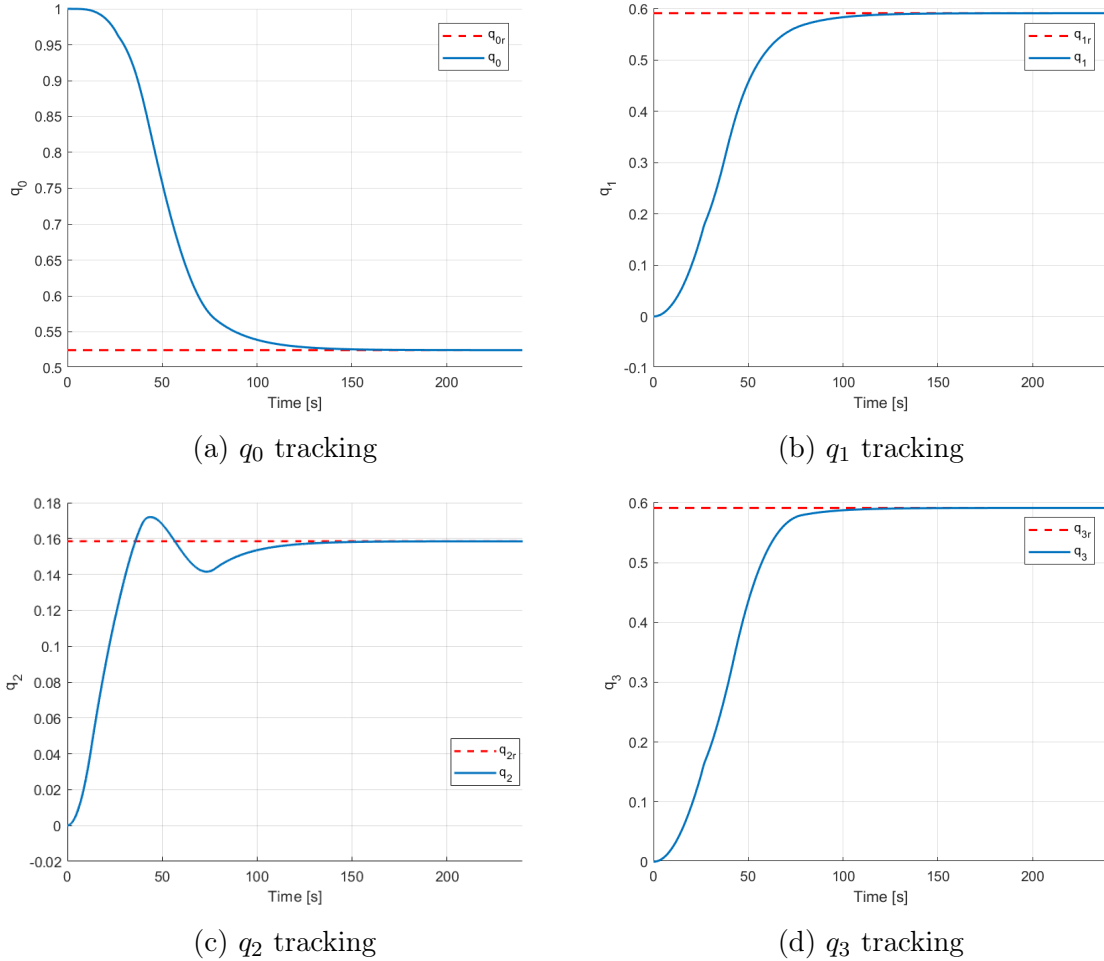


Figure 6.10: Quaternions tracking with moving manipulator

Fig. 6.10 shows that the reaching time is about 120 s, just as Scenario 1. Of course the manipulator's movements introduce some differences, like the overshoot in q_2

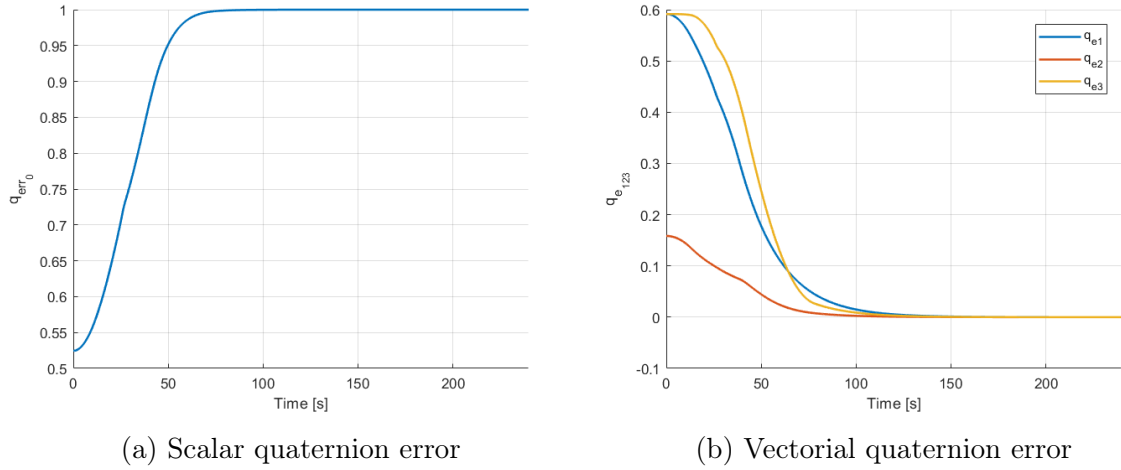


Figure 6.11: Quaternions tracking error

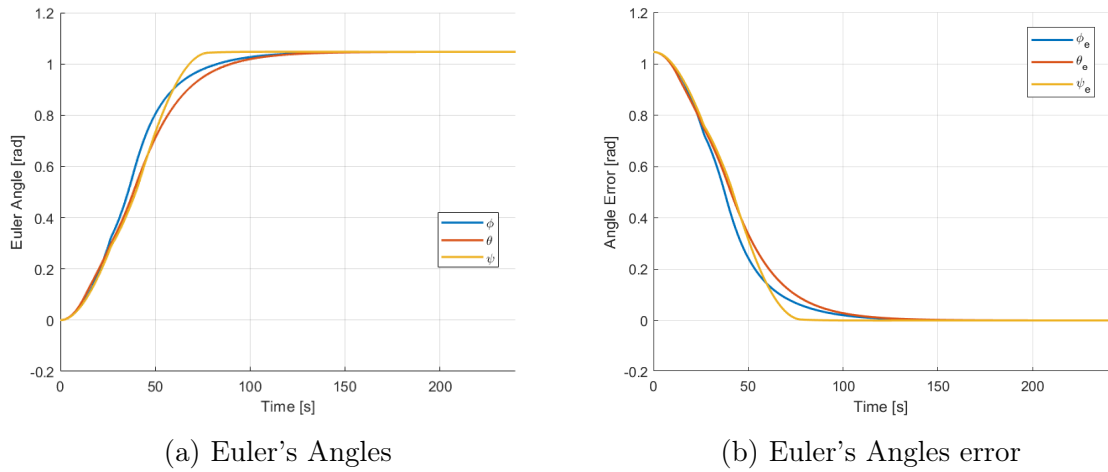


Figure 6.12: Euler' Angles

When comparing the Euler's angle error in Fig. 6.12b with the ones for the Scenario 1 in Fig. there is practically no difference, exception made for some disturbances around $t=25\text{ s}$, from the point of view of the Base-satellite's attitude.

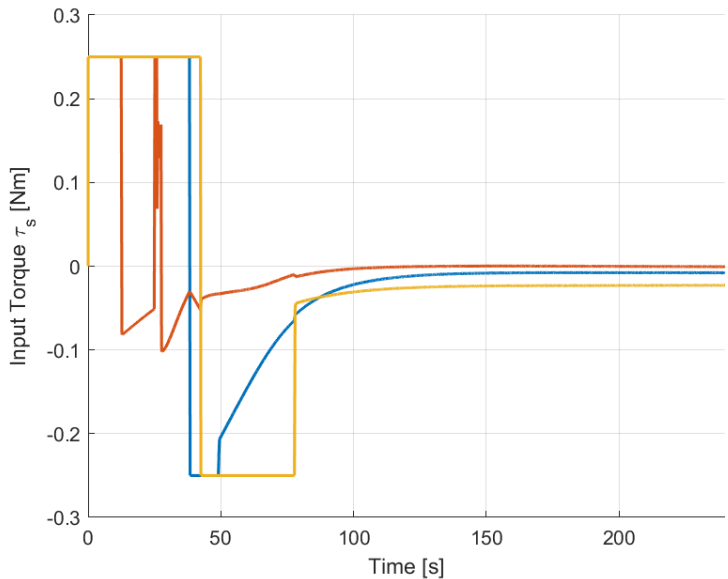


Figure 6.13: Torque input by SMC controller

To keep the satellite’s attitude on track, the command signal is perturbed at $t = 25\text{ s}$ because of the manipulator’s move start. After the manipulator’s start, the command activity returns normal and very similar to the one in Scenario 1 shown, in Fig. 6.4.

6.4 Earth-Observation-like Mission

To better validate the proposed control strategy, a real scenario is simulated. In this mission scenario, intended for Earth-Observation, the base-satellite has to track a attitude path while periodic manipulator's movements are performed.

The quaternion tracking is reported in Fig.6.14.

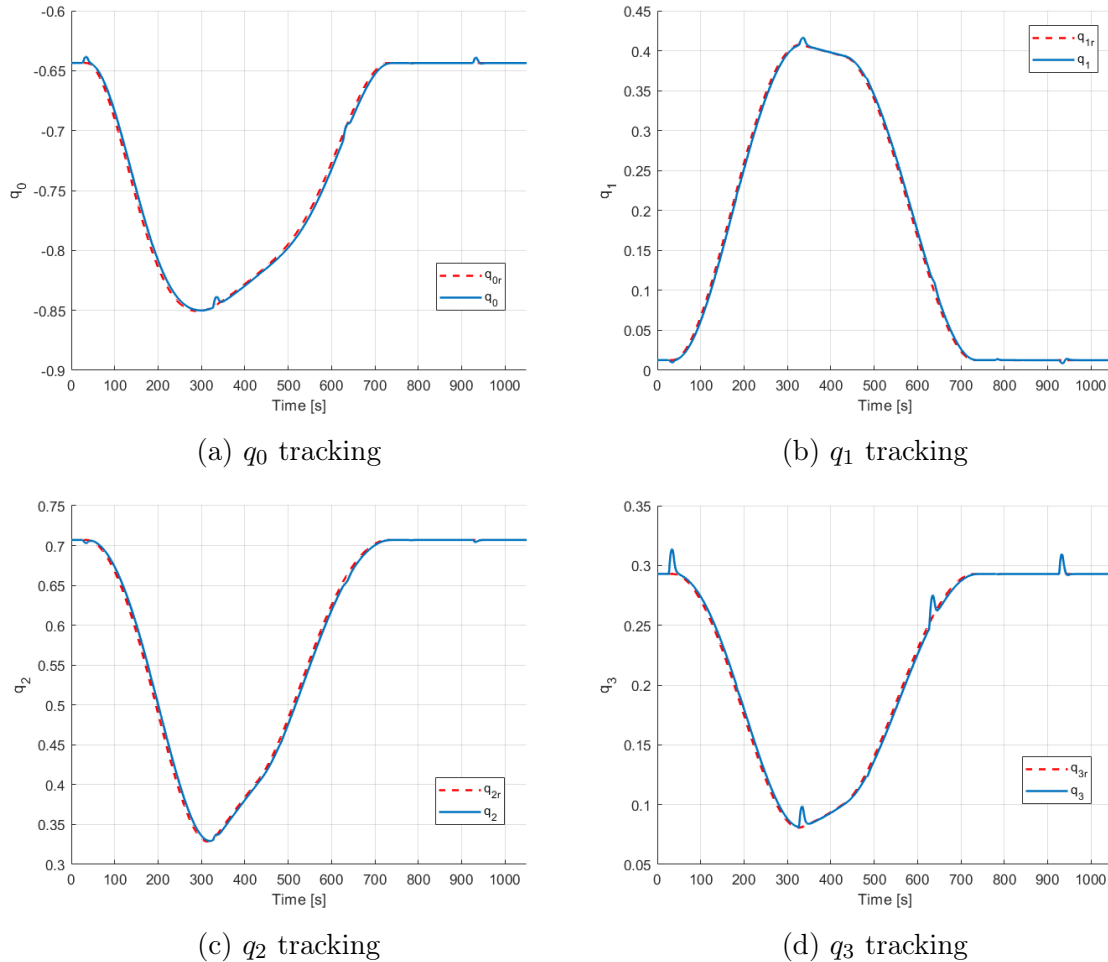
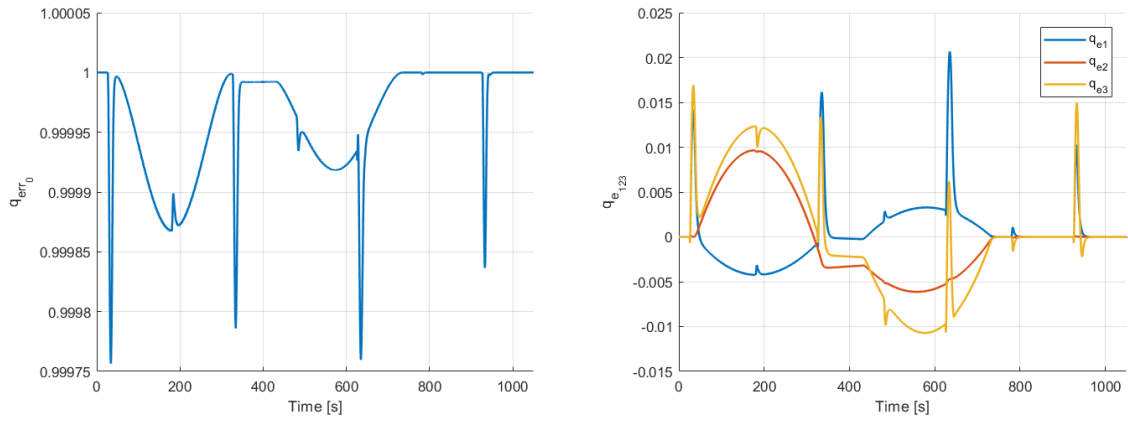


Figure 6.14: Quaternions tracking with moving manipulator

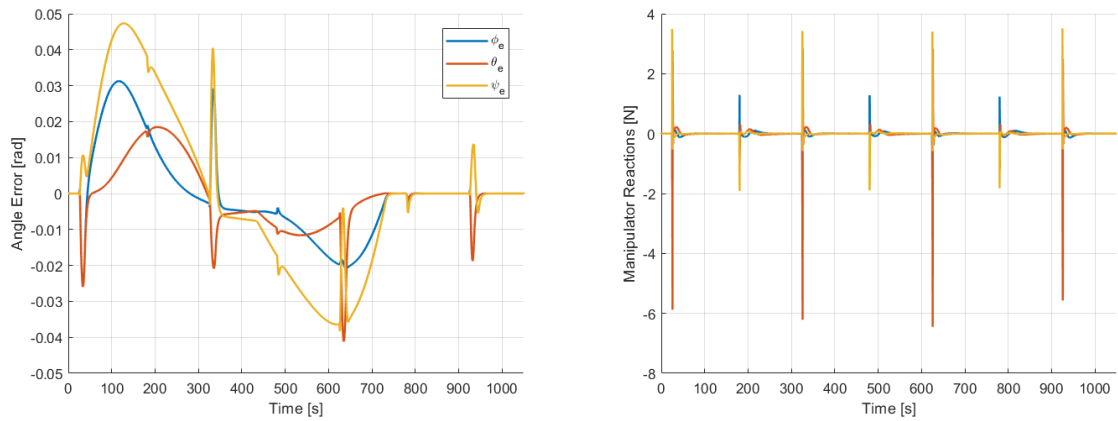
It's possible to notice in Fig. 6.14 some peaks corresponding to the manipulator's movements. The reference quaternion, represented in dashed red lines, is very well tracked from the base-satellite's SMC. When a peak occurs, the controller is able to compensate the disturbances and bring the actual attitude to the desired one.



(a) Quaternion error, scalar component (b) Quaternion error, vectorial component

Figure 6.15: Quaternions tracking error

The Euler's angles tracking error shown in Fig. ?? in the show a bounded error even when there are some pulse-like behavior. The error are bounded in $\pm 0.05 \text{ rad}$ range (i.e. $\pm 2.86^\circ$).



(a) Euler's angles error (b) Manipulator's reaction torques

Figure 6.16: Euler's angles tracking error and manipulator's disturbances

As discussed in Section 5.3, the manipulator's reactions include non-compensated linear forces on the base-satellite in all the three directions. Hence, the base-satellite is subjected to linear accelerations, resulting in linear movements. Fig 6.17 shows the satellite's position has been moved of several meters in all directions since simulation start $t = 0$ s until the end $t = 1100$ s.

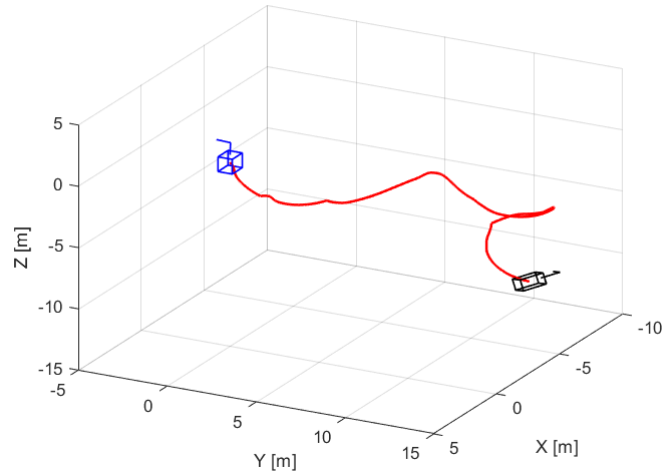


Figure 6.17: Satellite's displacement trajectory due to manipulator reactions

As comparison, a second maneuver in which the manipulator is considered in a fixed position is performed. The Euler's Angles errors for both cases are reported in Fig. 6.18.

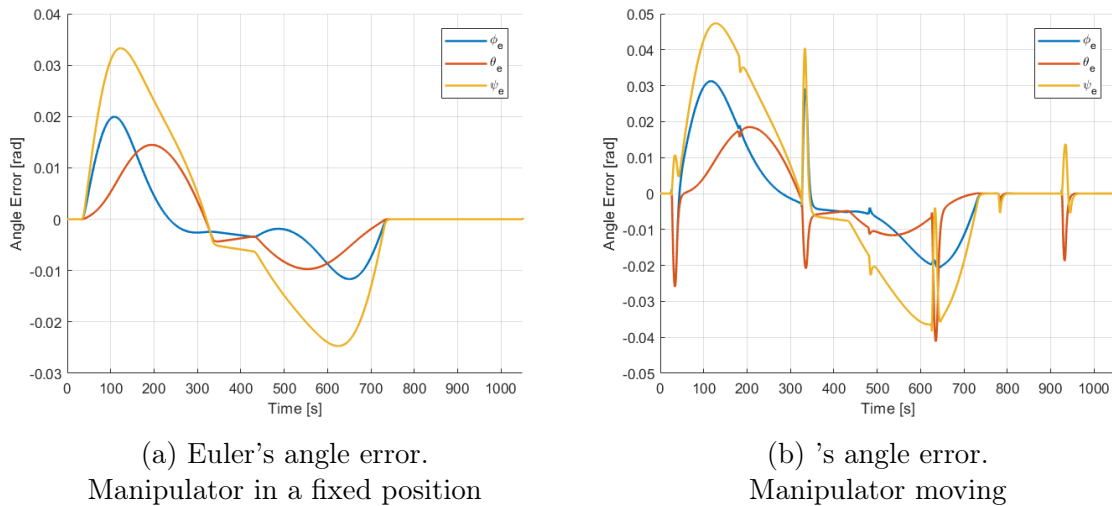


Figure 6.18: Euler's Angles tracking errors comparison

Comparing Fig6.18a and Fig6.18b, it's possible to see that the tracking error where the moving manipulator, is higher in magnitude but still bounded to small angles, about ± 0.05 rad or $\pm 2.86^\circ$

Conclusions

The main objective of this thesis was to design an attitude controller able to withstand a manipulator's reactions, affecting the base-satellite's orientation. An additional controller for the manipulator, in the joints' space, has been designed as well, in order to perform better simulations and better analyze the reactions behavior. The manipulator has been considered to have a mass equal to the 10% of the base-satellite, which is enough to produce considerable torques and forces.

The proposed control approach employed two different controllers for the two subsystems. Hence, the coupling term H_{0m} presents in Section 5.2 has been not considered from the control point of view. This fact could suggest that the controller strategy isn't the optimal one, since some important terms have been neglected. Despite this fact the control strategy is able to bound the reactions' effects, as the simulations performed on MATLAB and Simulink have shown.

The simulations have proven that the two-channel control design is able to track and maintain the desired attitude even in different scenarios where both the manipulator and the base-satellite were moving. The satellite's attitude is well tracked even in the presence of the manipulator's reactions. This is also due to the smooth manipulator's performance. An issue that can be easily solved is the one affecting the position in space. The simulations have shown that the reaction forces can reach up to 6N in magnitude and there is no way to compensate them. However, this is not a concern from an attitude control point of view but it should be considered in a orbit controller.

This two-channel control succeeded in compensating the reactions on the satellite, as simulations have shown. A consideration is that a more precise, unified controller considering the coupling terms would definitely have better performances. The reasons are that if a two-channel controller, neglecting a relevant part of the plant's dynamics, is able to perform so well, then a more detailed controller should be able to handle even better the overall system, maybe with better manipulator's performances.

As reported before, the manipulator's controller has been designed in the joint space. A very interesting future works could be the design of the system's Inverse Kinematics. Some considerations have been made in this thesis, like considering the base-satellite as a sort of special joint. Such Inverse Kinematics should allow, starting from a certain pose for the manipulator's End Effector, using the attitude and manipulator's controllers and, most likely an orbital one, to get the correct base-satellite's attitude and position for the joints' angles. This would be a remarkable achievement, also considering that the manipulator considered is redundant.

In order to design a final servicing satellite, given the huge tasks such satellite may performs, other future works are plenty. Some considerable ones are reported:

1. A rendezvous and docking Guidance Navigation and Control system should be designed in order to approach the customer's satellite and act on it. This system should also consider the case where obstacles are present on the path,
2. Since in-orbit servicing would require several tools depending from the scenario, such manipulator's tools have to be designed in order to be performant, redundant and exchangeable. Also, introducing some tools on the manipulator's End-Effector changes its kinematics at some level thus, several direct kinematics have to be derived depending on the tool in use. This would also lead to the development of path-planning for precise interactions between the service satellites and the customer's one.

Bibliography

- [1] O. Mitsushige *Motion control of the satellite mounted robot arm which assures satellite attitude stability* Acta Astronautica, 1997. 1
- [2] M. Oda *Attitude control experiments of a robot satellite* Journal of Spacecraft and Rockets, 2000. 1
- [3] Union of Concerned Scientist *UCS Satellite Database*. v, 2, 4
- [4] Henshaw, G. *Orbital Robotic Servicing* The International Workshop on On-Orbit Satellite Servicing, Oct. 2010 2
- [5] Lanius, R. and McCurdy, H. *Robots in Space* The Johns Hopkins University Press, 2008.
- [6] NASA, Goddard Space Flight Center *On-Orbit Satellite Servicing Study Project Report* Oct. 2010 2
- [7] Tatsch, A., Fitz-Coy, N., and Gladun, S. *On-orbit Servicing: A Brief Survey* Performance Metrics for Intelligent Systems Conference, August 2006, Gaithersburg, MD. 2, 7
- [8] J. Katz, D. W. Miller *Estimation and Control of Flexible Space Structures for Autonomous On-Orbit Assembly* Massachusetts Institute of Technology, Jun. 2016 2
- [9] NASA *In-Space Robotic Manufacturing and Assembly (IRMA) Update for NAC TIE Committee* Nov. 2016 3
- [10] Oegerle, W. R., Purves, L. R., Budinoff, J. G., Moe, R. V., Carnahan, T. M., Evans, D. C., and Kim, C. K. *Concept for a large scalable space telescope: in-space assembly* Society of Photo-Optical Instrumentation Engineers, Jul. 2006
- [11] Akin, D. L., Roberts, B., Roderick, S., Smith, W., and Henriette, J.-M. *MORPHbots: Lightweight Modular Self- Reconfigurable Robotics for Space Assembly, Inspection, and Servicing* AIAA Space, San Jose, CA, September 2006 3
- [12] S. Eckersleya, C. Saundersa, D. Goodinga, M. Sweetinga, C. Whitinga, M. Ferrisa, J. Frienda, L. Forwarda, G. Agliettib, A. Nanjangudb, P. Blackerb, C. Underwoodb, C. Bridgesb, P. Biancoc *In-Orbit Assembly of Large Spacecraft Using Small Spacecraft and Innovative Technologies* Massachusetts Institute of Technology, Jun. 2016 v, 3
- [13] R. Skomorohov, C, Welch, A.M. Hein *n-orbit Spacecraft Manufacturing: Near-Term Business Cases Individual Project Report* HAL, Sept. 2016 3
- [14] NASA *The Geometry of Success: Archinaut Project Conducts First Large-Scale Additive Manufacturing Build in Space-like Environment* Aug. 2017 3

- [15] *DOCTOR: Developing On-orbit Servicing Concepts, Technology Options, and Roadmap* Final Report of the International Space University, 2007
- [16] United Nations *Technical Report on Space Debris* UN, New York, 1999 4
- [17] NASA *Restore-L Robotic Servicing Mission*. 2010. v, 4
- [18] Sullivan, B. *Technical and Economic Feasibility of Telerobotic On-Orbit Satellite Servicing* University of Maryland, 2005 4, 6
- [19] NASA *NASA's Robotic Refueling Demo Set to Jumpstart Expanded Capabilities in Space* Jen., 2017 4
- [20] Kaiser, C., Sjöberg, F., Delcura, J. M., and Eilertsen, B. *SMART-OLEV—An orbital life extension vehicle for servicing commercial spacecrafts in GEO* Touching Humanity - Space for Improving Quality of Life. Selected Proceedings of the 58th International Astronautical Federation Congress, Hyderabad, India, Sep. 2007 v, 5
- [21] Y. Shtessel, C. Edwards, L. Fridman, A. Levant *Sliding Mode Control and Observer*. Birkhauser, 2010 6
- [22] G. Bartolini, A. Ferrara, and E. Usai *Chattering avoidance by second-order sliding mode control*. IEEE Transactions on Automatic Control, Feb 1998. v, 6
- [23] F. Landis Markley John, L. Crassidis *Fundamentals of Spacecraft Attitude Determination and Control*. Springer, 2014 6
- [24] E. Canuto, C. Novara, L. Massotti, D. Carlucci, C. P. Montenegro *Spacecraft Dynamic and Control. The Embedded Model Control Approach*. Butterworth-Heinemann 9
- [25] United States Naval Observatory *Astronomical Almanac Online 2018. Selected Astronomical Constants*. USNO, Washington, DC, USA 11
13, 14, 15, 18
- [26] S. R. Crews II. *Increasing slew performances of reaction wheel attitude control systems*. Monterey, CA, USA:Naval Postgraduate School, Sep. 2013. 14
- [27] M. Wilde, S.K. Choon, A. Grompone, M. Romano. *Equation of Motion of Free-Floating Spacecraft-Manipulator System:An Engineer's Tutorial*. Florida Institute of Technology, Naval Postgraduate School, Apr. 2018. 14
- [28] J. Shah, S.S. Rattan, B.C. Nakra. *Dynamic Analysis of two link robot manipulator for control design using computed torque control*. International Journal of Reseach in Computer Applications and Robots, Jen. 2015. v, 16, 17
- [29] Joseph Virgili-Llop *SPART Documentation. Release 0.2.0*. Feb. 2018. 20, 27, 28
- [30] B. Siciliano, L. Sciavicco, L. Villani, G. Oriolo. *Robotics. Modelling, Planning and Control*. Springer, 2010. 21
26, 33
- [31] Honeywell *Constellation Series Reaction Wheels*. Dec. 2003 v, 27, 30, 33
36